

Risk-based compromise solutions between beam and column bending capacities for progressive collapse mitigation in reinforced concrete frames

Lucas da Rosa Ribeiro^a, Lucas Araújo Rodrigues da Silva^a, André Teófilo Beck^a, Fulvio Parisi^{b,*}

^a Dept. of Structural Engineering, University of São Paulo, Av. Trabalhador São-carlense, 400, 13566-590, São Carlos, SP, Brazil

^b Dept. of Structures for Engineering and Architecture, University of Naples Federico II, Via Claudio, 21, 80125, Naples, Italy

ARTICLE INFO

Keywords:

Progressive collapse
Reinforced concrete buildings
Risk-based optimization
Structural robustness
Robustness-oriented design

ABSTRACT

Optimal design of double-span beams under middle support loss depends significantly on beam end constraints. Fully clamped constraints favor catenary action, reducing optimal beam cross-sections. To provide a more realistic optimization of beam and column designs, a complete two-dimensional reinforced concrete (RC) frame is addressed herein, under various ground-floor column loss scenarios. This allows simulating realistic lateral drifts on top of columns, and the failure of beams and adjacent columns. Nonlinear finite element analysis via OpenSees is carried out, allowing Vierendeel, compressive arch and catenary actions to be accurately predicted under large displacements. Risk is quantified in terms of total expected progressive collapse cost, so design optimization finds the best tradeoff between construction costs and expected consequences of failure. Cost-effective mitigation strategies against progressive collapse are shown to depend strongly on column loss probabilities, but also on the balance between beam and column flexural capacities. For square column cross-sections, increasing beam stiffness to activate compressive arch action is observed to be more cost-effective than increasing column stiffness to produce catenary action. Conversely, rectangular columns with higher stiffness produce smaller drifts, promoting optimal square beam cross-sections to develop satisfactory catenary action.

1. Introduction

Disproportionate progressive collapse relates to a disproportion between damage caused by an initial failure and the total area affected by its propagation [1]. When abnormal loads cause failure of a small part of the structure, a cascade of subsequent failures may be triggered, affecting a much larger portion of the structure [2]. As a local failure initiates the collapse of nearby elements, further progressive failures are triggered, culminating in a chain reaction and large-scale collapse [3]. Such severe events are often triggered by threats like fires, earthquakes, flooding, accidental impact and terrorist attacks [4,5]. Robustness characterizes a structure's insensitivity, or small sensitivity, to initial damage and/or to disproportionate damage propagation [4–8].

Structural robustness is typically promoted by enhancing Alternative Load Paths (ALPs) [6,7]. The Alternative Path Method (APM)

* Corresponding author.

E-mail addresses: lucasribeiro@usp.br (L.R. Ribeiro), araujolucasrs@usp.br (L.A. Rodrigues da Silva), atbeck@sc.usp.br (A.T. Beck), fulvio.parisi@unina.it (F. Parisi).

<https://doi.org/10.1016/j.job.2025.113713>

Received 4 April 2025; Received in revised form 21 July 2025; Accepted 6 August 2025

Available online 9 August 2025

2352-7102/© 2025 The Authors. Published by Elsevier Ltd. This is an open access article under the CC BY-NC-ND license (<http://creativecommons.org/licenses/by-nc-nd/4.0/>).

is a design framework for progressive collapse mitigation, in which structural robustness is enhanced by producing ALPs. Herein, initial damage relates to the sudden loss of a single column caused by an unspecified hazard (threat-independent approach), following the usual APM guideline framework [8,9] and hazard assumptions from Beck et al. [10,11].

In reinforced concrete (RC) frames, the ALPs rely on complementary resisting mechanisms whose activation depends on the remaining beams and columns: flexural action (FA), Vierendeel action (VA), compressive arch action (CAA), and catenary action (CA) [5]. These mechanisms depend on which column is lost, as CAA and CA require adjacent columns on both sides to be activated. Therefore, loss of an external column relies solely on FA and VA [12]. For an inner missing column scenario, FA, CAA and CA can be directly related to the frame's force vs displacement behavior (Fig. 1).

Flexural action involves elastic behavior, concrete cracking, and steel yielding at the beam ends (point A in Fig. 1a). Beyond this point, increasing rotations at the beam-column joints push the beam ends outward. If the adjacent columns provide adequate anchorage and lateral confinement, compressive axial forces develop in the double-span beam (Fig. 1b), characterizing CAA, with peak resistance related to advanced rebar yielding and concrete crushing (point B in Fig. 1a). A snap-through may then occur, with its severity depending on beam depth and adjacent column stiffness. If the structure withstands these stages, the two-bay beam enters CA as its axial load shifts to tension (Fig. 1c), being considered the last defense against progressive collapse (point C in Fig. 1a) [13].

Ultimate capacity may be defined at CAA and CA stages, with CA being usually preferable due to its greater ductility. Both mechanisms rely on detailing of beams and columns, span lengths, and material properties [14–18]. As some design decisions favor CAA capacity while others influence the CA capacity, risk-based optimization can be used to define the most cost-effective solution, as well as pre-defined structural requirements, costs of robustness-targeted strengthening and expected costs of progressive collapse [13, 19,20].

For instance, Ribeiro et al. [21] show that an RC beam detailing that prioritizes CA capacity is the optimal risk-based solution for a fully clamped double-span beam, or a beam with infinite lateral confinement. To explore a more realistic system, this study addresses the optimal risk-based design of a planar RC frame under multiple scenarios of ground-floor column loss, targeting the optimal design of all beams and columns. Unlike the idealized setup in Ref. [21], the current model captures the finite stiffness and deformation of columns, which directly influence the development of resisting mechanisms such as CAA and catenary action [16,17]. Additionally, column dimensions and column reinforcement are now included as design variables, enabling the investigation of trade-offs and flexural compromises between beams and columns. These extensions make the current framework significantly more complex and representative of actual structural behavior, thereby extending the scope and applicability of the previous study [21]. While this study addresses a single five story by six bay perimeter frame, other frame aspect ratios are addressed in a companion paper [62].

In recent years, significant advancements have been made in developing mitigation strategies for progressive collapse, particularly in enhancing structural redundancy, continuity, and robustness. These include the use of fuse elements, energy-dissipating components, segmented structural layouts, and performance-based design approaches aimed at improving post-damage load redistribution capacities [6,14,22–26]. The integration of innovative detailing methods and alternative reinforcement strategies has also shown potential to improve structural performance under column loss scenarios. While the present work focuses on trade-offs between construction cost and collapse performance through optimization of beam and column stiffness in planar RC frames, recent state of the art strategies are valuable contributions to the broader field of collapse mitigation and an important direction for future extensions of this research.

2. Case-study structure

The planar RC frame tested by Yu and Tan [16] is the object of study (Fig. 2). By addressing multiple scenarios of single column loss via pushdown analysis [27], it is possible to investigate how the complex interaction between distinct structural elements reflects on the optimal risk-based results. The following initial damage cases are considered: external column loss (ECL), penultimate column loss (PCL), antepenultimate column loss (ACL), and middle column loss (MCL). Based on [16], nominal values for dead and live loads are 7.1 kN/m^2 and 4.8 kN/m^2 , respectively, with an additional load of 2 kN/m to account for non-structural exterior components. It is

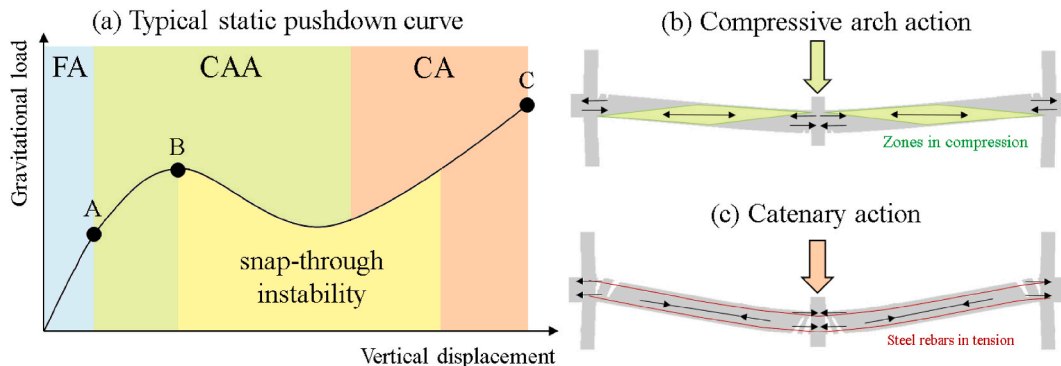


Fig. 1. Resisting mechanisms in a (zoomed-in) two-bay RC beam in a multistory frame.

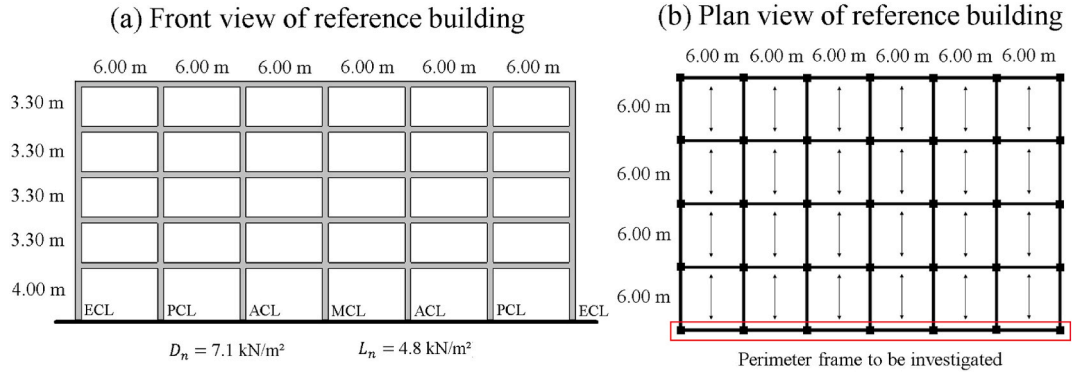


Fig. 2. Reference RC structure and studied frame.

further assumed that the structure is located in a non-seismic region, as seismic hazards are beyond the scope of the present investigation.

All columns at the ground floor are subjected to a probability of sudden removal given by p_{LD} . Unidirectional floor slabs are considered. Hence, the perimeter frame gets floor loads from one side only. If an inner frame was addressed, two floor loads would be added to the beams, so greater optimal reinforcements would be expected. However, real life occurrences of progressive collapse due to terrorist attacks, for instance, shows that facade columns at the ground floor are more usual targets.

As discussed by Rodrigues da Silva et al. [28], identifying critical failure sequences to simplify the problem is fundamental. Therefore, based on [11], 2 types of collapse spread after loss of a single column are assumed: (a) upward propagation due to beam failure; and (b) lateral propagation due to column failure. When the first set of adjacent columns fail, beam span length increases,

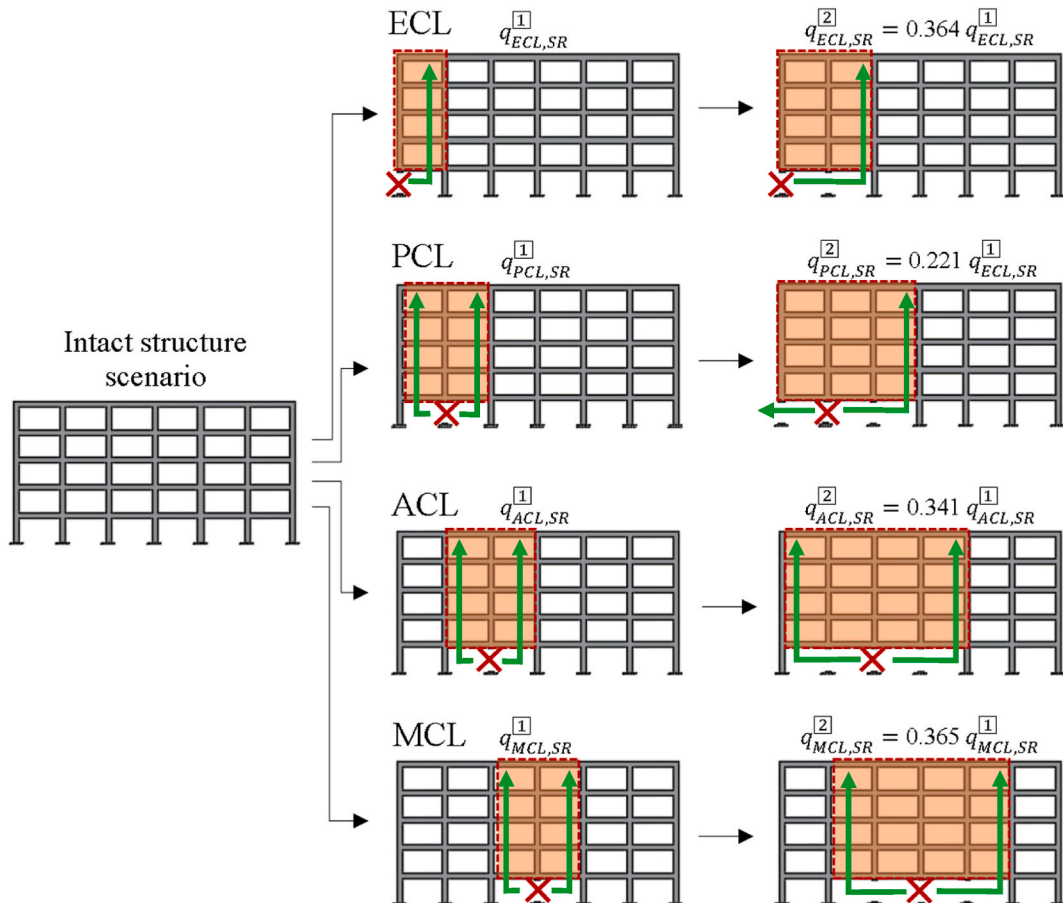


Fig. 3. Critical failure sequences (green arrows) and potential damaged extent (in red) for reference frame.

significantly increasing bending moments and axial forces on the new set of adjacent columns. For the reference frame studied herein, this leads to probabilities of beam failure of ~ 0.99 when the first set of adjacent columns is lost. Therefore, as shown in Fig. 3, only the 1st and 2nd lateral propagation stages are addressed, with horizontal collapse propagation turning to an upward propagation of greater damage extent after failure of the first set of adjacent columns.

To simplify the cascading failure analysis, second-stage events are considered as function of first-stage failures. In Fig. 3, $q_{iCL,SR}^j$ relates to the ultimate CA capacity for the i^{th} column loss scenario and j^{th} stage of lateral spread. A uniform sample of 200 points (based on Table 1) was used to estimate these ultimate capacities for all stages and scenarios, allowing the beam ultimate capacity at 2nd stage to be written in terms of the 1st stage capacity ($CoV \approx 5\%$). These relations are used when computing the limit states of the increased beam span in case of adjacent column failure (to be later introduced).

Note that penultimate column loss (PCL) has $q_{PCL,SR}^2$ written in terms of $q_{ECL,SR}^1$, as its 2nd stage cantilever shape resembles a hypothetical 3rd stage of ECL. Besides, beam shear demands at 2nd stage are estimated as ‘increased beam length \times load’, which are then compared to the shear capacity (limit states to be described).

2.1. Sensitivity analysis





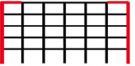
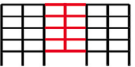
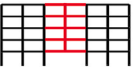

Fig. 4 shows a beam sensitivity analysis for the reference frame under MCL. To emphasize the relevance of column stiffness, two conditions are shown in this figure: (a) fully clamped two-bay beam, as in Refs. [16,21]; and (b) whole frame. For results in Fig. 4, columns are assumed identical to Ref. [16], and only beam parameters are varied: cross-section depth (h_B), bottom and top rebar diameter (ϕ_B and ϕ_T , with 3 rebars per layer), concrete strength (f_c') and rebar yielding strength (f_y). The reference beam (black lines in Fig. 4) shares the seismic-detailing design reported in Ref. [16].

By comparing the models, static pushdown analysis [27] for the RC frame shows less pronounced snap-through compared to the fully clamped RC beam. Thus, pushdown behavior may change drastically for beam-only modeling and whole frame simulation. While a reduced beam depth (h_B) increases ultimate capacity at CA in a beam with clamped ends, the opposite is observed when addressing the whole frame (Fig. 4a and b, respectively). Such large differences can be explained by the horizontal drift at the adjacent columns, namely: a large drift for the whole frame model, and negligible drift for fully clamped beams.

Ultimate capacities at CAA and CA are greater for the fully clamped beam model, as maximum resistance against horizontal drift is present in this case. By contrast, whole frame modeling leads to greater ductility in terms of vertical drift due to adjacent columns having lower stiffness. For both modeling strategies, ultimate capacity at CAA and CA is proportional to the rebar diameter of both layers, but with increased values of ϕ_T leading to the greatest resistance values at CA (Fig. 4c–f).

Table 1

List of failure modes, limit state functions and assumed damaged areas.

Case	Failure mode	k	Limit state function	Damaged area
Intact structure (I)	Large deflection (SE)	5	$g_{I,SE}(\mathbf{x}) = \delta_{lim} - \delta(q_I)$	
	Positive bending (BM)	30	$g_{I,BM}(\mathbf{x}) = M_{RM} - M_M(q_I)$	
	Negative bending (BE)	30	$g_{I,BE}(\mathbf{x}) = M_{RE} - M_E(q_I)$	
	Shear failure (SH)	60	$g_{I,SH}(\mathbf{x}) = V_R - V(q_I)$	
	Column failure (CO)	60	$g_{I,COL}(\mathbf{x}) = R(N_R, M_R) - S(N_{SI}, M_{SI})$	
Column loss (CL_i)	Steel rebar rupture (SR)	40	$g_{CL_i,SR}(\mathbf{x}) = q_{CL_i,SR} - q_{CL}$	
	Shear failure (SH)	60	$g_{CL_i,SH}(\mathbf{x}) = V_R - V(q_{CL})$	
	Column failure (CO)	80	$g_{CL_i,COL}(\mathbf{x}) = R(N_R, M_R) - S(N_{SCL_i}, M_{SCL_i})$	

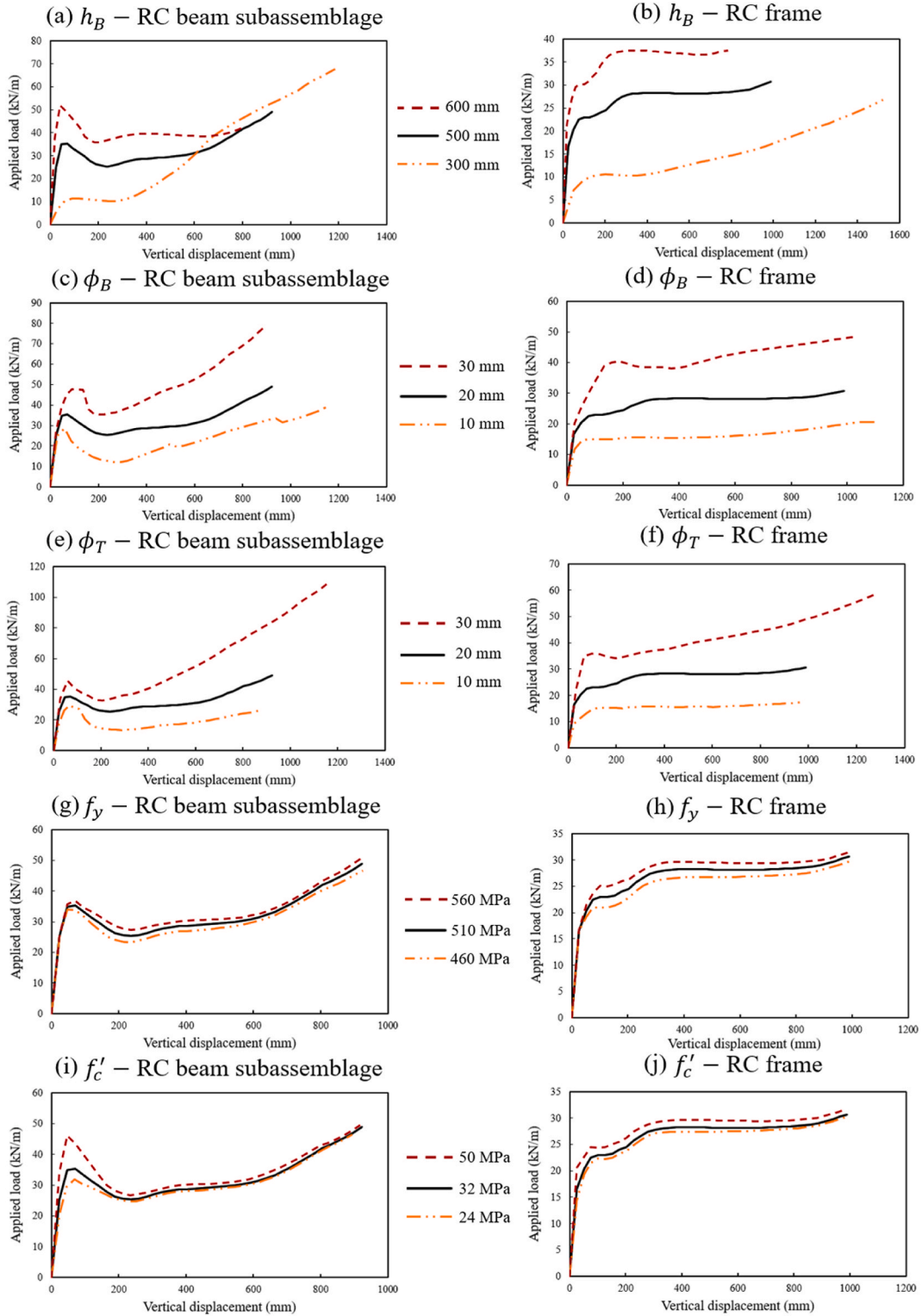


Fig. 4. Load vs displacement responses: fully clamped beam (left) and frame model (right).

When addressing yield strength f_y , the end of FA (onset of CAA) is the main feature affected, as the pushdown behavior past this point is unaffected (Fig. 4g and h). Additionally, concrete strength f'_c has a reduced role in the pushdown behavior of the RC frame model, since the increase in CAA capacity is not as relevant as for the beam subassemblage model (Fig. 4i and j). Based on these results,

significant differences are expected in the optimal risk-based design of a whole frame system, in comparison to a fully clamped beam subassemblage [21].

3. Methodology

This work addresses the optimal risk-based design of a conventional RC frame under gravity loads and column loss scenarios, aiming to understand how optimal design of beams and columns adapts to mitigate progressive collapse. Redistribution-type progressive collapse due to single column loss is addressed, and only intrinsic resisting mechanisms are considered. Hence, the main strategy for progressive collapse mitigation consists on enhancing existing ALPs via APM design, as done in the usual guideline framework. In this study, only a primary RC frame supporting unidirectional floor slabs is addressed, for which 3D and slab effects can be neglected. Design variables in the optimization problem are cross-sectional dimensions and reinforcement ratios (longitudinal and transversal).

Under multiple hazards, progressive collapse probability $P[C]$ can be computed as [29]:

$$P[C] = \sum_H \sum_{LD} P[C|LD, H] P[LD|H] P[H] \quad (1)$$

where: $P[H]$ is the probability of hazard occurrence; $P[LD|H]$ is the conditional probability of local damage given H ; and $P[C|LD, H]$ is the conditional probability of collapse given LD and H .

To focus on system behavior, Beck et al. [10,11] addressed Eq. (1) assuming the (fifty-year) probability of local damage $p_{LD} = \sum_H P[LD|H] P[H]$ as an independent term, accounting for epistemic uncertainty in potential abnormal loading scenarios leading to local damage. The authors showed that p_{LD} is the main parameter controlling the decision whether a specific building should be strengthened or not. Thus, the authors identified the local damage probability threshold p_{LD}^h , a break-even point which makes the additional cost of APM strengthening equal to the reduction in expected cost of progressive collapse failure. When $p_{LD} > p_{LD}^h$, it is cost-effective to strengthen the structure to mitigate progressive collapse. The authors show similar results for a threat-dependent approach involving blast loading [30]. For any particular building, p_{LD} is estimated in a risk assessment considering building location, surroundings, ownership and use, and all potential hazards leading to the local damage considered [11].

Herein p_{LD} is treated as an independent parameter ranging between $p_{LD}^{min} = 5 \times 10^{-6}$ and 1 (in a lifetime of 50 years), covering scenarios where the threat of local damage is negligible up to very significant threats. The lower bound p_{LD}^{min} relates to the 50-year lifespan equivalent to the “de minimis” annual probability $p = 10^{-7}$ [31].

3.1. General framework

Herein, risk-based optimization involves a vector of design variables \mathbf{d} , including beam and column cross sections and reinforcement ratios, and a vector of random variables (RVs) \mathbf{X} , encompassing uncertainty in dead and live loads, material strengths and member dimensions. Continuous design variables are the beam depth h_B , beam rebar diameter (bottom ϕ_B and top ϕ_T layers), beam stirrup spacing s_t , column size h_C (squared cross section), and diameter of column rebars ϕ_C . Hence, $\mathbf{d} = \{h_B, \phi_B, \phi_T, s_t, h_C, \phi_C\}$.

The design domain \mathcal{D} contains the mean values of some of the RVs in the sampling domain \mathcal{S} ; hence, $\mathcal{D} \subset \mathcal{S}$. Vector \mathcal{D} has a smaller dimension than vector \mathcal{S} , as some RVs are not considered as design variables, e.g. yielding strength, dead load, live loads, and model error. Design variables are conveniently considered as the means of RVs in order to: (a) ensure a more robust uncertainty modeling; and (b) allow use of the same sample to estimate failure probabilities for all optimal candidates (more details in Section 3.3). The adopted framework relies on four pillars and four sample sets, which are integrated according to Fig. 5:

- risk-based optimization: total expected costs, given by cost of construction and expected costs of failure, are minimized for each p_{LD} using Firefly Algorithm [32];
- reliability analysis: to compute expected costs of failure, probability of occurrence for each failure mode is estimated by Weighted Average Simulation (WASM) [33,34];
- structural modeling: for each sample point, structural response is obtained via nonlinear static analysis based on the Finite Element Method (FEM) using OpenSees software [35];

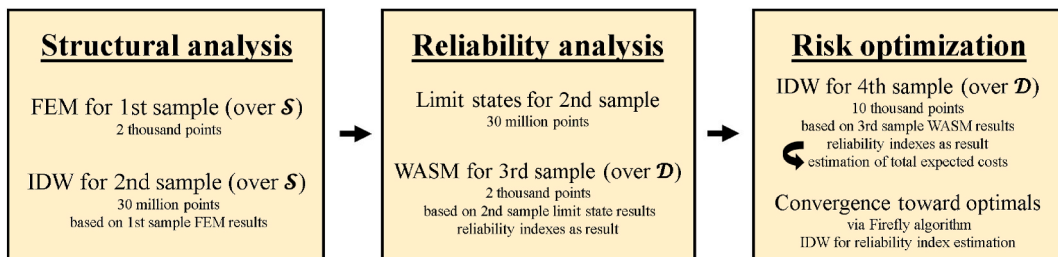


Fig. 5. Proposed framework.

- (d) interpolation: as integrating structural and reliability analyses has a huge computational cost, the simplified yet accurate Inverse Distance Weighting (IDW) scheme [36] is used to hasten these stages, making the proposed risk optimization a feasible process.

For each sample set, the chosen number of points is based on convergence analyses made across \mathcal{S} and \mathcal{D} . Latin Hypercube Sampling (LHS) [37–39] is used to create a 1st uniform sample set across the sampling domain \mathcal{S} , containing all the problem's RVs. FEM is used to realistically address structural behavior for the intact structure and for each column loss scenario.

A 2nd and significantly larger sample set is then created via LHS across \mathcal{S} , but now structural behavior is quickly interpolated via IDW (CoV $\leq 5\%$). To ensure convergence in reliability analysis, the 2nd sample set must reach dozens of millions of sample points, so it is unfeasible to get their structural behavior estimated directly via FEM. More complex surrogate techniques, such as ordinary kriging, were observed to be too slow for the hundreds of outputs needed to estimate the force–displacement pushdown curve (including internal forces of interest) for each sample point and for each column loss scenario.

Each sample point in the larger 2nd sample set has its limit state function $G = R - D$, where R is the resistance of the structure and D is the demand, i.e. the effects of loads, on the structure. For each column loss scenario, the force–displacement curve can be estimated using eight key points related to fixed values of beam rebar strain ε_s , as follows: 0, 0.002, 0.01, 0.05, 0.10, 0.15, 0.20, and 0.25. At each key point, vertical drift, applied load, and internal forces of interest are inferred via FEM (1st sample set) or estimated via IDW (2nd sample set). This enables a less conservative approach for dynamic effects (introduced in Section 3.4), and an efficient and accurate parameter estimation at any ε_s within feasible computational time, meeting the requirements of this study.

Then, a 3rd sample set is created via LHS across the design domain \mathcal{D} . For each design sample point, the previous (2nd) large RV sample set and their limit state results are used as basis to compute the probability of occurrence and respective reliability index for all failure modes via WASM. A 4th sample set is then created via LHS across \mathcal{D} for risk-based optimization purposes (initial set of fireflies in the Firefly Algorithm). The reliability indices for the 4th sample points are quickly (and accurately) estimated via IDW interpolation in terms of the support points previously evaluated in reliability analysis (3rd sample set).

As the iterative optimization process advances, candidate solutions converge towards the optimum (most cost-effective solution), and for each candidate the failure probabilities are quickly (and accurately) interpolated via IDW still based on the 3rd sample set results. Although the probability of failure modes related to column loss scenarios is conditional on threat probability, the same reliability index IDW support points (3rd sample set) can be used for all p_{LD} values. This is possible due to the threat-independent approach proposed by Beck et al. [10], which separates the mechanical system behavior in the progressive collapse phase from the hazards and conditional local damage probabilities.

3.2. Optimization procedure

The objective function to be minimized is the total expected cost C_{TE} , which addresses manufacturing costs and expected costs of all failure modes of the intact structure and of each column loss scenario (Eq. (2)). Since a symmetric frame is addressed, ECL, PCL and ACL are considered twice when computing C_{TE} . Additional life-cycle costs could certainly be included; however, this study considers only those related to construction and expected failure losses, in line with prior work [21], to specifically address the consequences of progressive collapse. The focus is on the trade-off between construction cost and expected failure cost as a starting point for risk-informed structural optimization. This narrowed scope enables a tractable framework that isolates the direct economic implications of robust design strategies. While broader life-cycle and sustainability-related costs are indeed important [40], their inclusion would extend beyond the core objective of this paper. Future work will incorporate such holistic evaluations as the framework is expanded.

$$C_{TE}(\mathbf{d}) = C_M(\mathbf{d}) + \sum_{i=1}^{NIF} k_i C_{MAi} p_{fi} + \sum_{k=1}^{NCL} \sum_{j=1}^{NCLF} k_j C_{MAj} p_{fj} p_{LDk} \quad (2)$$

where $C_M(\mathbf{d})$ is the frame construction cost; NIF and $NCLF$ are the number of failure modes for intact and damaged structure, respectively; NCL is the number of scenarios of single column loss; k is a failure consequence factor, accounting for direct and indirect losses; p_f is the probability of occurrence; and C_{MA} is the construction cost of the damaged frame area affected by the addressed failure mode. In Eq. (2), the term p_{LDk} relates to the local damage probability p_{LD} previously defined in Section 3, corresponding to the k th column loss scenario.

The manufacturing cost of the affected area C_{MA} varies depending on the failure mode and column loss scenario, as depicted in Table 1. Each failure mode is assumed to damage a specific portion of the frame, and the construction cost of this specific part is used as reference when computing its expected cost of failure. To compute C_M , costs of formwork, workmanship, concrete and steel are accounted for as in Ref. [21], but with updated reference values of July 2024 [41,42]. For each failure mode, k and C_{MA} are shown in Table 1. Under normal load condition, the expected cost for any given failure mode is $C_{EF}^I(\mathbf{X}, \mathbf{d}) = k C_{MA} p_f$, whereas the expected cost for each column loss condition is $C_{EF}^{ICL}(\mathbf{X}, \mathbf{d}) = k C_{MA} p_f p_{LD}$. Although C_{MA} depends on \mathbf{d} and p_f is a function of both \mathbf{X} and \mathbf{d} , this is omitted in Eq. (2) for clarity purposes.

Multipliers k reflect the severity of a failure mode in terms of the construction cost C_{MA} related to the area affected by the system damage state [10,11,21]. Values range according to the analysis made by Marchand and Stevens [43], which compares the cost of construction to the cost of collapse of the Alfred P. Murrah Federal Building, World Trade Center and Pentagon. Hence, less severe

failure modes, such as serviceability failure (in terms of allowable deflection) and bending failure (cross-section plastification due to rebar yielding and/or concrete peak strength) have smaller values of k , while brittle shear and column failures have greater values. Therefore, k is assumed as shown in Table 1. Yet, higher failure cost multipliers could be employed for critical or strategic buildings.

As done in Ref. [21], rebar rupture in CA is considered the less severe failure mode for the column loss scenarios. This is because shear failure and adjacent column failure prevent the full development of the pushdown response, causing collapse before the beam reaches its ultimate capacity, representing a more critical, premature failure. In contrast, rebar rupture indicates that the structure has fully utilized its deformation and material strength capacity, without earlier failures interrupting the load path. Although rebar rupture remains undesirable due to the potential for extensive damage, it is treated as the least critical among the evaluated failure modes. Shear failure is assumed to compromise a similar portion of the structure but at lower load and displacement thresholds, while adjacent column failure impacts an even larger area prematurely. Thus, as whole frame modeling for squared-section columns leads to a negligible snap-through (Fig. 4), no penalization is needed to ensure CA capacity above the CAA capacity.

The cost-benefit analysis is done by solving the optimization problem given by:

$$\begin{aligned} &\text{for a given } p_{LD} \\ &\text{find } \mathbf{d}^* \\ &\text{which minimizes } C_{TE}(\mathbf{d}) \\ &\text{subject to } \mathbf{d} \in \mathcal{D} \end{aligned} \quad (3)$$

Since rebar diameter is optimized, a fixed number of 3 rebars at each beam layer and 8 rebars for the squared-section columns is adopted, as shown in Fig. 6. Since multiple columns are subject to sudden loss, p_{LD} in Eq. (2) is addressed in two different manners: a) p_{LD} relates to a *specific* column loss, for which progressive collapse is studied individually; b) p_{LD} relates to the loss of *any* column, with local damage probability per column $p_{LDcol} = p_{LD}/(\text{number of target columns})$. This allows consideration of how each scenario individually influences the optimal design, and how they compete for the strengthening budget.

3.3. Limit states and reliability analysis

Table 1 illustrates all failure modes addressed in this study, inclusive of limit state functions, damaged areas and failure-cost multiplication factors.

Beam failure in the intact scenario refers to a single continuous beam, since it is unlikely that live load reaches its 50-year extreme value in all stories simultaneously. Column failure in the intact scenario is considered only at the top corner due to the greater bending moments and low compressive forces in these regions. Even with a 20-mm eccentricity, column failure does not occur at the frame's base, even for the weakest possible column within \mathcal{D} . Although MCL is chosen to illustrate the damaged areas in Table 1, the actual damage extent depends on which column is lost, as shown in Fig. 3.

Variables in Table 1 are as follows:

- ✓ q_I and q_{CL} are the distributed loads for intact (I) and column loss (CL) scenarios, respectively;
- ✓ δ_{lim} is beam displacement threshold of 15 mm [44];
- ✓ $\delta(q_I)$ is the beam vertical drift in the intact frame;
- ✓ M_{RM} and M_{RE} relate to beam bending capacity at midspan and ends, respectively [44];
- ✓ $M_M(q_I)$ and $M_E(q_I)$ are the beam bending demands at midspan and ends, respectively;
- ✓ V_R is the beam shear capacity [44];
- ✓ $V(q_I)$ and $V(q_{CL})$ are the shear demands in the beams for intact and damaged structure, respectively;

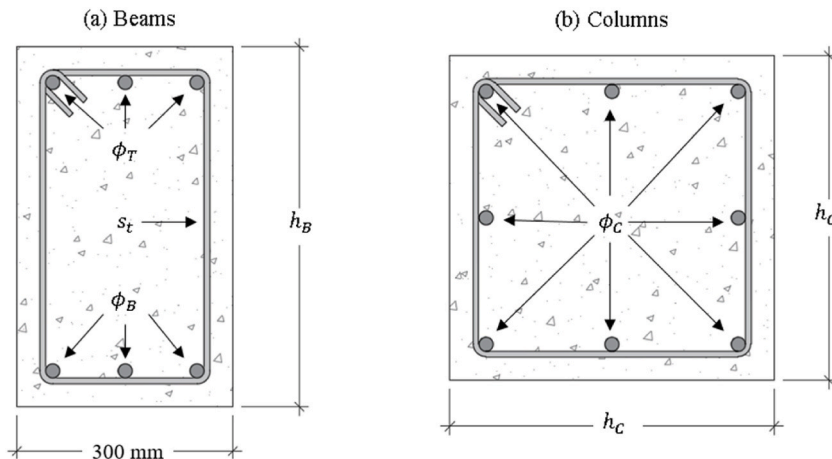


Fig. 6. Cross-sections to be optimized in the RC frame.

- ✓ $R(N_R, M_R)$ relates to the columns axial force vs bending moment resisting envelope [44];
- ✓ $S(N_{SI}, M_{SI})$ and $S(N_{SCLi}, M_{SCLi})$ are the columns axial force vs bending moment demands for intact and damaged frame, respectively;
- ✓ $q_{CLi,SR}$ is the beam capacity in terms of top layer rebar rupture at the adjacent beam-column joints.

Table 2 shows the adopted uncertainty modeling. Boundary values for \mathcal{S} are chosen in terms of $\mu \pm 2\sigma$ for each random variable, where μ is the vector of mean values and σ is the vector of standard deviations. Although this range is not optimal for computing small probabilities via WASM, it is accurate enough for our risk optimization purposes. Indeed, probabilities below 10^{-4} relate to negligible expected costs of failure, so high accuracy for smaller probability values is not necessary.

3.4. Structural analysis

OpenSees is used to conduct finite element (FE) structural analysis. Each span is discretized in 5 fiber displacement-based finite elements (3 Gauss-Lobatto integration points in each), being three FEs for the member itself and one at both ends to represent the beam-column joint regions. Praxedes [13] shows the efficiency of this approach in terms of minimal refinement level and agreement with experimental static pushdown curves, even though the beam-column joints are not explicitly modelled.

Corotational transformation is used for all members to account for the expected large geometrical nonlinearities. To avoid convergence issues, member cross-sections were meshed through 200 fibers for confined concrete and 10 fibers for each face of unconfined concrete cover. Static bay pushdown analysis [27] is conducted with a displacement-based integrator using Krylov-Newton method to solve the nonlinear problem (tolerance set to 10^{-5}). An initial increment size of 1 mm is adopted, whereas an adaptive algorithm is used to increase or decrease the step size depending on the lack or need of convergence improvement, respectively.

Since bay pushdown analysis is conducted, two load steps are adopted: (a) nominal values of both dead and live loads are applied over all beam spans, as well as the self-weight of all structural members, by means of distributed line loads; (b) if beam rebar rupture does not occur in the first stage (possible case for slight reinforcement beam configurations), an increasing distributed line load is applied over the beam spans of interest until rebar rupture is attained.

The modified Park-Kent model [50] is used to model confined and unconfined concrete behavior in compression, and the multilinear model from fib Model Code [51] serves as reference for concrete in tension. As shown in Figure A.1a (Appendix), all main parameters from both models are used as inputs for the ‘concretewBeta’ model available in OpenSees. Some parameters, such as K , ε_{20u} and ε_{20c} are outputs from the reference concrete model [50], inferred from cross-section geometry, material strengths and stirrup detailing. Although commonly used for RC truss modeling, ‘concretewBeta’ is able to satisfactorily represent softening and residual stresses both in tension and compression. Residual stress of tensile concrete is negligible in the applications of this study, but assuming a residual value of $0.01 f_{cm}$ is enough to avoid convergence issues related to singular stiffness matrixes.

Rebar behavior is represented by the ‘ReinforcingSteel’ model available in OpenSees, which realistically encompasses the linear elastic region, the yield plateau, strain hardening, and strain softening which are expected for typical steel reinforcements (Figure A.1b in Appendix). Usual bilinear models are not used because they may lead to unrealistic rebar stresses for advanced stages of CA. Hence, the chosen rebar model produces realistic results in close agreement with experimental data.

Dynamic effects related to a sudden column loss can be represented by explicit dynamic analysis, Dynamic Amplification Factors (DAF, conservative approach), or by Energy Equivalent Method (EEM). As a pragmatic solution is enabled by EEM, this approach is chosen herein. EEM consists of a balance between kinetic energy, external work and internal deformation energy, where a pseudo-

Table 2
Uncertainty modeling.

Category	RV	Distribution	Mean value and range	Standard deviation	Coefficient of variation	Reference
Geometry	Beam depth (h_B)	Normal	To be optimized* [300, 600] mm	1 mm	–	[45]
	Bottom rebar diameter (ϕ_B)	Normal	To be optimized* [12,30] mm	–	0.05	[45]
	Top rebar diameter (ϕ_T)	Normal	To be optimized* [12,30] mm	–	0.05	[45]
	Stirrup spacing (s_r)	Normal	To be optimized* [100, 200] mm	–	0.05 (assumed)	–
	Column size (h_C)	Normal	To be optimized* [400, 600] mm	1 mm	–	[45]
	Column rebar diameter (ϕ_C)	Normal	To be optimized* [12,30] mm	–	0.05	[45]
Material	Concrete strength (f_c)	Lognormal	32 MPa	–	0.12	[46,47]
	Rebar yield strength (f_y)	Normal	510 MPa	–	0.05	[46]
	Ultimate steel strain (ε_{su})	Normal	0.13 (normal ductility) 0.20 (high ductility)	–	0.14	[46,48]
Loads	Dead load (D)	Normal	$1.05 D_n$	–	0.10	[49]
	50-year live load (L_{50})	Gumbel	$1.00 L_n$	–	0.25	[49]
	a.p.t. live load (L_{apt})	Gamma	$0.25 I_n$	–	0.55	[49]
Capacity model	Model error (M_E)	Lognormal	1.101	0.187	–	This study

static pushdown curve is obtained by integration of the static pushdown curve [52–55]. For simplification, energy dissipation from other sources, such as heat and plastic strains, is neglected, leading to small discrepancies in the dynamic estimation. Herein, the pseudo-pushdown curve is estimated via EEM at all sample points, for which key points of the static pushdown curve are obtained directly via FEM or interpolated via IDW (1st and 2nd sample sets of Fig. 5, respectively).

4. Results

This section presents the optimal risk-based results obtained by analyzing multiple progressive collapse scenarios. The study evaluates the structural response under different column loss cases, including ECL, PCL, ACL, and MCL. As mentioned in Section 3.2, the local damage able to trigger progressive collapse is addressed by p_{LD} , which may refer to: (a) loss of a specific column; or (b) individual loss of any column. Additionally, the intact structure scenario is considered to ensure that progressive collapse mitigation design does not compromise performance under Normal Loading Conditions (NLC). By systematically addressing these scenarios, it becomes possible to understand how the complex interaction between distinct structural elements influences the optimal design and how ultimate capacity is prioritized.

Four strengthening strategies to enhance structural robustness are examined, resulting from the combination of two parameter variations. One parameter is the extent of strengthening, which includes the options of strengthening the entire frame or only the first two stories. The other parameter is longitudinal rebar ductility: low-ductility rebars, with a strain limit mean of 0.13 (as in Refs. [13, 16]), are compared to high-ductility rebars, which exhibit a more reasonable limit strain of 0.20, commonly used in studies of structural robustness. The results provide insight into how these parameters affect the structural system's ability to withstand column loss while maintaining cost-effective design solutions.

For each case the optimal risk-based design is investigated under increasing values of p_{LD} . Firefly algorithm is used to solve Eq. (3),

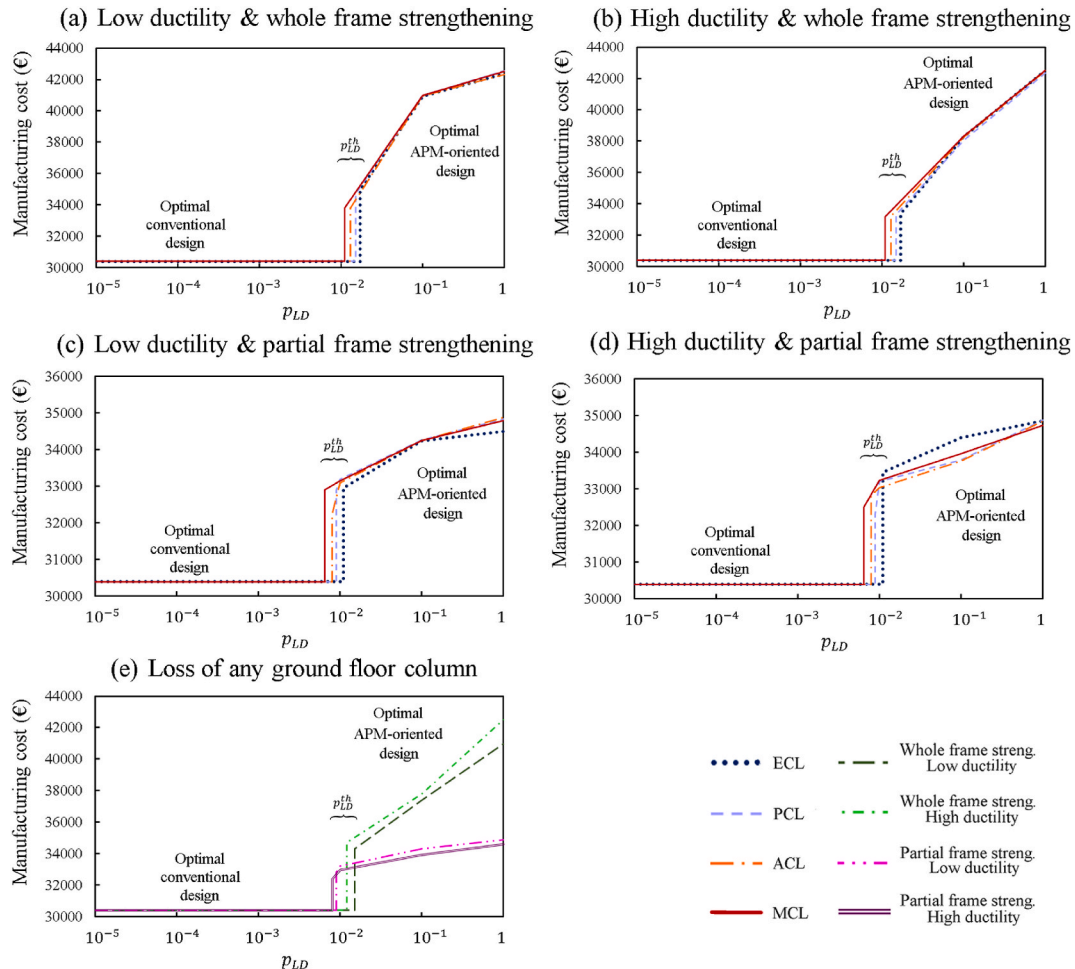


Fig. 7. Optimum manufacturing cost C_M as function of column loss probability p_{LD} .

relying on 10 optimization runs for each p_{LD} value, 100 iterations per run, and 40 fireflies. Despite multiple optimization runs for each scenario and each p_{LD} value, only the mean results are shown, as all cases are characterized by small dispersion, with all CoVs remaining below 5 %.

4.1. Optimal design solutions and column-loss probability threshold

In the following, superscript $(\cdot)^*$ indicates the optimal value of the given design variable. Fig. 7 shows the evolution of optimal manufacturing cost C_M for all column loss scenarios and strengthening decisions investigated, with p_{LD} ranging from 5×10^{-6} (p_{LD}^{min}) to 1. Only C_M is shown to highlight how the optimal solution changes from a conventional design to an APM-oriented design as p_{LD} grows. Tables in Appendix A show in greater detail the optimal results for all cases and strengthening approaches, including optimal C_{TE} values found for all p_{LD} .

The plots in Fig. 7 show two sets of optimal solutions, divided by the threshold local damage probability p_{LD}^{th} (approximately 10^{-2} in this study). In the first set, entitled “conventional design” and obtained for small p_{LD} , optimal solutions favor behavior under normal loading conditions (NLC); in the second set, entitled “APM-oriented design” and obtained for large p_{LD} , optimal solutions adapt to address progressive collapse under column loss scenarios.

The local damage probability threshold p_{LD}^{th} is the break-even point, for which the costs of APM strengthening nearly match the reduction in expected costs of progressive collapse. Therefore, p_{LD}^{th} indicates an indifference in the objective function, where two near-optimal solutions coexist: one prioritizes alternative load paths with reduced expected costs of progressive collapse, while the other aligns with conventional design under normal loads, with reduced construction cost [10,11,21].

Both solutions have similar total expected costs at p_{LD}^{th} : one with smaller construction cost but increased expected costs of progressive collapse (NLC-oriented), and the other with greater construction costs but reduced expected costs of collapse propagation (APM-oriented). This explains the sudden increase in C_M at p_{LD}^{th} in the plots of Fig. 7. As p_{LD} increases past p_{LD}^{th} , greater APM strengthening is needed to compensate increasing probabilities of progressive collapse. Hence, C_M increases past the corresponding p_{LD}^{th} value as additional progressive collapse strengthening becomes cost-effective.

Optimal conventional beam design (for $p_{LD} < p_{LD}^{th}$) is similar to that found in Ref. [21], being controlled by bending failure at the beam ends ($\beta_{I,BE}^* \approx 3.2$) and column failure at the frame’s top corner ($\beta_{I,CO}^* \approx 3.4$) (Figure A.2 in Appendix A). Based on Table 1, symbols BE and CO relate to beam negative bending and column failure, respectively, both for the intact scenario. Optimal APM beam design is similar for all cases: maximum beam depth (600 mm) and reinforcement ratios of 0.82 % for bottom rebars, 1.03 % for top rebars, and 0.25 % for stirrups at higher p_{LD} values. Optimal APM design has lower beam safety margins for both steel rupture or shear failure, depending on the strengthening strategy and p_{LD} value (Figures A.3 and A.4 in Appendix A). Nonetheless, p_{LD}^{th} is characterized by $\beta_{iCL,SR}^*$ reaching a minimum of 2.33.

Tables A.1 to A.5 in Appendix A, in conjunction with Fig. 7, show that when p_{LD} relates to the sudden loss of any column, optimal APM beam design solutions are similar to those found for specific column loss. Yet, optimal column designs are similar for all cases and p_{LD} values (see discussion in Section 4.3). Partial frame strengthening reduces C_M and C_{TE} in ~ 19 %, and the gap between optimal C_M and C_{TE} is greater for low ductility rebars. High-ductility rebars provide a slight economy in terms of C_{TE} , even when it leads to greater C_M . Partial frame strengthening makes APM design cost-effective for smaller threat probabilities. Yet, gas explosions at the upper floors, for instance, are not addressed by this strategy.

The optimal APM solutions obtained herein are consistently related to literature findings. For instance: beams with greater depth promote CAA capacity [14]; greater optimal rebar reinforcements in APM designs promote increase in frame ultimate capacity [17]; however, optimal over reinforced beams are related to slightly decreased flexural capacity and earlier mobilization of CA [56]; top reinforcement ratio is always greater in optimal progressive collapse-resistant beam design, as progressive collapse is characterized by rupture of the top rebar layers at the adjacent beam column-joints [17]; strengthening the two first floors is shown to be a cost-effective solution for low-rise frames [57].

Assuming loss of any ground-floor column leads to optimal APM design being cost-effective for $10^{-3} < p_{LD}^{th} < 10^{-2}$ for partial frame strengthening. This relates to probabilities per column p_{LDcol}^{th} ranging from $\sim 1.428 \times 10^{-4}$ to $\sim 1.428 \times 10^{-3}$. Assuming that such probability per column p_{LDcol}^{th} does not change, overall p_{LD}^{th} for loss of any ground-floor column increases for higher number of columns. Hence, passive measures that reduce the number of potential target columns may have better cost-benefit than addressing an APM design that covers multiple scenarios of single column loss [58].

External column loss scenarios are the most critical, as neither CAA nor CA can be mobilized, making the structure entirely dependent on VA. Consequently, reinforcement becomes expensive as more steel rebar area is needed to achieve enough capacity for the expected abnormal loading, so APM design is cost-effective only for higher threat probabilities ($p_{LD}^{th} > 10^{-2}$). Penultimate column loss scenarios are the next most critical. Although CAA and CA can develop, lateral restraint is unbalanced due to a single adjacent column on one side, leading to significant axial-flexural demands in the outermost column. In general, the deeper the lost column is within the frame, the less critical the scenario becomes, as mobilization of CAA and CA actions improve.

Optimal APM design has increased safety margins against brittle shear and column failures, while also ensuring a minimum safety margin against ductile steel rupture in CA action (i.e., the least bad failure mode) and all NLC failure modes (Figures A.2-A.4 in Appendix A). Resistance factors show that flexural capacity for optimal APM designs is at least twice the flexural capacity for optimal conventional design. Ultimate capacity in terms of rebar rupture is also shown to become more than double, regardless of column loss scenario, for columns of square cross-sections (Figure A.5 in Appendix A).

4.2. Optimal tradeoffs between ultimate load-bearing capacity and frame ductility

A detailed look at risk-based optimum solutions for frame beams (shown in Appendix A) reveals that these solutions explore a “Pareto front” of compromises between ultimate capacity and frame ductility (Fig. 4). As shown in the sensitivity analysis of Fig. 4, increasing h_B increases the ultimate load-bearing capacity at the expense of decreasing the overall frame ductility (large displacements) for the same amount of rebar ductility (ϵ_{su}). Hence, optimizing h_B while ensuring a thorough usage of confined concrete beyond softening and steel rebars up to their rupture reveals a Pareto front of compromise solutions, as shown in Fig. 8.

In terms of h_B , each static pushdown curve is a solution of full usage of each material, and the set of all solutions corresponds to a Pareto frontier in terms of ϵ_{su} . It is noted that multi-objective solutions are not addressed herein. Fig. 8 reveals the different points of compromise which are explored in the risk-based optimization, which looks for a good balance between construction costs and expected costs of failure.

In this example, the optimal $h_B^* = 600$ mm obtained for all cases reflects a preference for greater load carrying capacity, in detriment of frame ductility. Although both CAA and CA capacities are enhanced, the expected abnormal loading is within the frame’s CAA resisting mechanism, so CA is not developed in case of sudden column loss. This might compromise the time needed for building evacuation in case of abnormal loading greater than expected, so the balance between ultimate capacity and frame ductility requires further investigations. Yet, constraints in terms of ductility requirements could be adopted to ensure minimal evacuation time.

Optimal beam designs with maximum load capacity and minimal vertical drifts ($h_B^* = 600$ mm) correspond to smaller tensile axial forces during CA stage, which in turn reduces the bending moments transmitted to adjacent columns. Hence, beam depth is shown to be a highly relevant design variable due to its direct effect on strength across 6 failure modes (SE, BM, BE, SH, and SR) and its indirect reduction in moment demand on columns. Reducing h_B^* in favor of greater frame ductility would require additional longitudinal and transversal reinforcements, as well as significantly larger column cross sections, to achieve similar safety margins against all failure modes. This approach, however, is shown to be cost-ineffective for the studied frame.

4.3. Optimal column design

As discussed in the previous section, optimal solutions relate to progressive collapse mitigation by means of CAA activation only (for the expected abnormal loading demands), with CA mobilization being avoided. Although CA allows maximum deployment of materials up to their limits, it is strongly related to the flexural demand on the adjacent columns (as discussed in Section 1 and depicted in Fig. 1). Resisting mechanisms in the beam spans above a lost column rely on the development of compressive and tensile axial forces (CAA and CA, respectively, all together with VA), which depend on the available horizontal restraint. In this study, RC columns of square section are the sole providers of this lateral confinement.

Load combination for accidental/extreme loading condition is given by $q_{CL} = 1.22(1.2D_n + 0.5L_n)$, with 1.22 being a common DAF value found between CAA and CA stages. This leads to 57 kN/m for the beam spans above a lost column, 47 kN/m in the non-affected beam spans, and 4.8 kN/m for column spans, so 2550 kN is roughly expected at the foot of the adjacent columns. When comparing to the resisting envelope of the optimal column designs (same for all cases and p_{LD} values), this axial demand is around 50 % of the

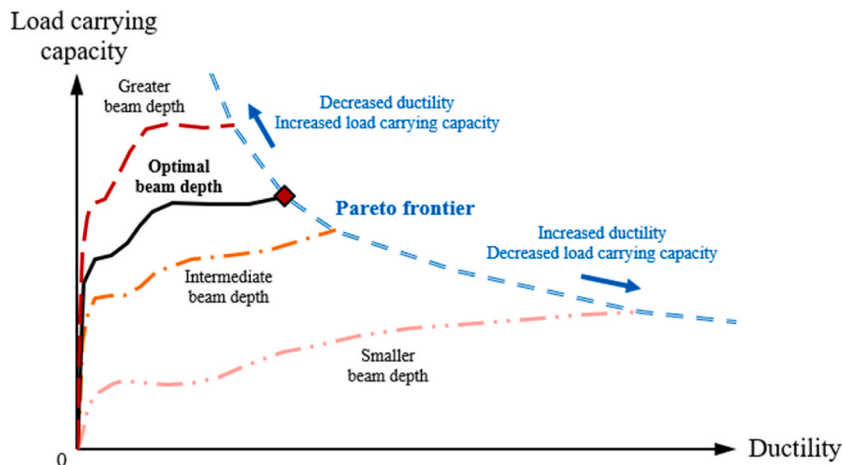


Fig. 8. Tradeoff between ultimate structural capacity and frame ductility.

columns' axial capacity, so the decisive factor behind the APM detailing is not an enhanced compressive demand. Due to VA, optimal column design relies on the significant bending moment demands caused by beams under CAA and CA. As tensile forces under CA may be significantly greater than compressive forces associated with CAA, greater flexural demands at the adjacent columns are expected when beams develop their CA.

4.3.1. External column loss (ECL)

Scenarios of external column loss are unable to trigger CAA and CA mechanisms due to a lack of bi-lateral restraint. Hence, load-carrying capacity relies on FA and VA, leading to minor impacts in bending demand on adjacent columns. Fig. 9 shows the resisting envelope for the 2nd set of optimum column designs, and the expected force vs moment demands (N–M diagram) obtained by FE analysis for 200 sample points. Each FE analysis addresses the same frame and the same 2nd set of optimum column designs, but with random combination of beam design variables across the design space \mathcal{D} . This allows the identification of the effects that weak, intermediate and stronger beams have over the N–M column demand.

For all sample points the resisting envelope encompasses the N–M demands of the adjacent columns. In this scenario, Vierendeel Action leads to compressive forces at the first floor, tensile forces at the uppermost floor, and a gradual transition from lower to upper floors, ensuring equilibrium for the hanging frame span. Those axial forces, which only develop due to the stiffness of the adjacent column, cause a flexural demand in it, with the frame being pushed inwards at the lower floors and pulled outwards at the upper floors. As shown in Fig. 9, a significant safety margin can be observed for the axial force–moment demand at the bottom of the adjacent column, which seems to be indifferent to the beam configuration. However, greater bending moments on top of the adjacent column can be observed for weaker beams, leading to smaller safety margins in this region. Nonetheless, this failure mode is related to column rebar yielding in tension, which has negligible impact over pushdown behavior, ultimate frame capacity, and structural robustness. Remaining floors in the hanging frame span have intermediate force–moment demands, so they are omitted for brevity. In addition, column tensile rebar yielding is common for the hanging column span, but with negligible implications.

4.3.2. Penultimate column loss (PCL)

Weak beams cause a major increase in column flexural demand for penultimate column loss, mainly at the outermost adjacent column (Fig. 10). Although CA is able to develop, the lateral restraint for the two-bay beams is unbalanced, causing distinct N–M demands over the adjacent columns. Weak beams have lower ultimate capacities, while experiencing larger vertical drifts (up to $\sim 4 h_B$) until rebar rupture happens.

This inherently leads to the development of greater axial forces in CA, which produce greater bending moments ($\sim 370\%$) on columns, resulting in the exceedance of the maximum bending capacity of the outermost column. This severely compromises the frame's pushdown behavior, leading to a premature collapse of a potentially larger portion of the frame. Despite domino-type progressive collapse not being addressed in this study, the propensity of its occurrence is visibly significant due to the overwhelming inward pull of the outer adjacent column.

The optimal APM column design is able to envelope all N–M demands of the inner-most adjacent column. For the outer adjacent columns, this only happens (barely) for the strong beams (greater h_B). Lower values of conditional reliability index $\beta_{PCL,CO}^* \approx 3.0$ are also justified by the aforementioned behavior (Figures A.3 and A.4 in Appendix A). Column flexural demand is greater in the adjacent column related to lower capacity of lateral restraint. Hence, the outermost adjacent column should be prioritized when addressing structural strengthening for columns lost closer to facades or building corners.

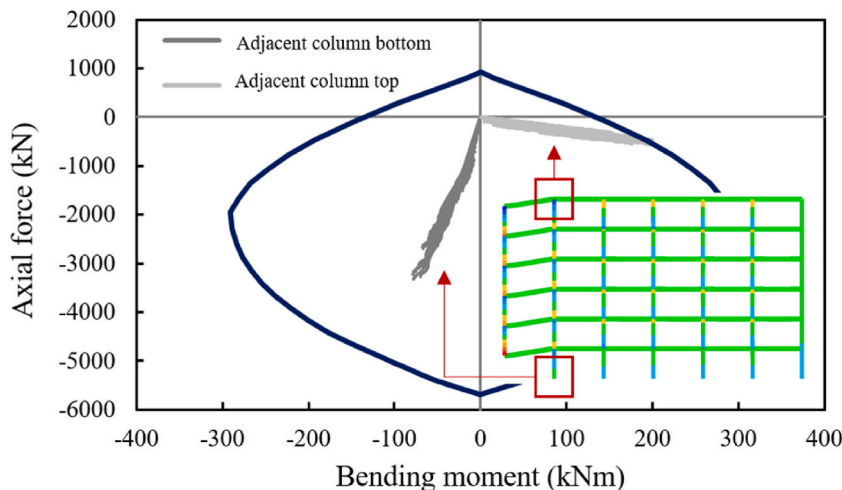


Fig. 9. Column failure assessment (N–M diagram) for external column loss scenario.

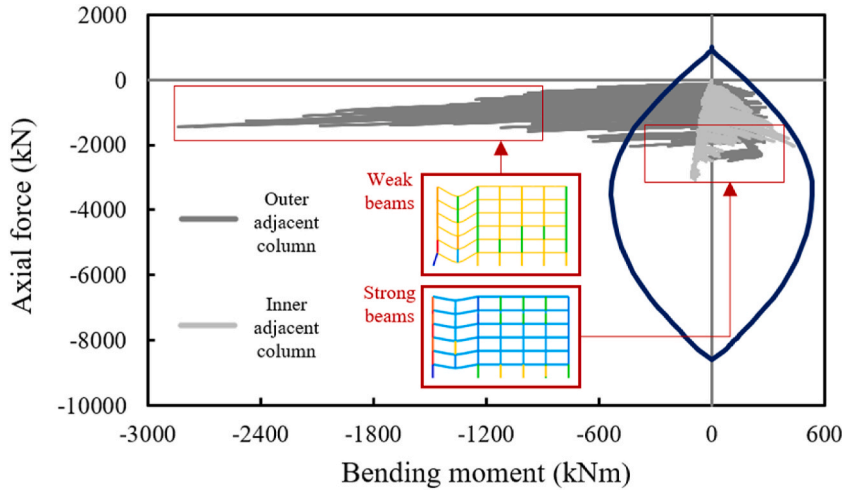


Fig. 10. Column failure assessment (N-M diagram) for penultimate column loss scenario.

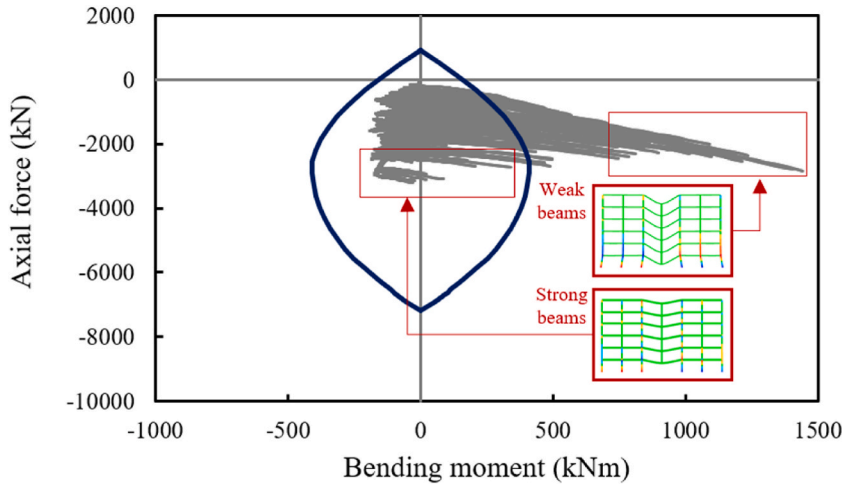


Fig. 11. Column failure assessment (N-M diagram) for middle column loss scenario.

4.3.3. Middle column loss (MCL)

Middle column loss leads to reduced values of flexural demand due to the balanced lateral restraints, but figures up to $\sim 190\%$ above the maximum flexural capacity are still possible for both adjacent columns (Fig. 11). For middle column loss, both adjacent columns require strong beams, as weak beam configurations can pull the entire frame inwards (domino-type collapse).

Despite middle column loss leading to smaller flexural demands in adjacent columns, its potential to affect the entire frame through zipper-type and domino-type collapses is greater compared to penultimate column loss. All optimal APM column designs found for each scenario have one aspect in common: ultimate axial capacity at least twice the maximum expected axial demand. Since column failure in redistribution-type progressive collapse is solely attributed to increased flexural demands, Fig. 12 shows that column cross-sections other than the classic square-shape could be more appropriate for APM design.

In Fig. 12, an illustrative rectangular cross-section with the same area and number of rebars is used, but with half of the rebars placed on each side (an unconventional arrangement adopted for clarity). This results in the same axial capacity, but the maximum flexural capacity is increased by approximately 150% . The new resisting envelope is able to accommodate greater bending demands, potentially providing greater safety margins for weaker beams.

Although the new rectangular section alters the N-M demands (hyperstatic frame), the previously calculated demands are kept for clarity. In addition, removing $3/4$ of the rebars in the compressed side seems to have a negligible negative effect in the tensioned side.

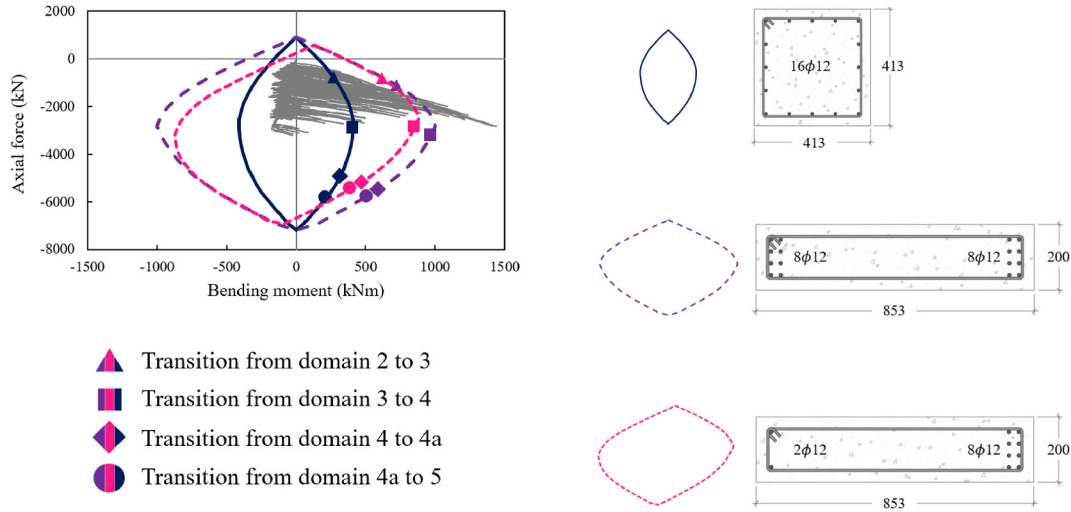


Fig. 12. Column failure assessment (N-M diagrams) for MCL with different cross-sections.

This could lead to optimal strengthening solutions with APM design paying off at lower threat probabilities and possibly allowing weaker beams (lower h_B) to be used, allowing CA mobilization.

By monitoring the neutral axis position across the column's resisting envelope, the thresholds between different flexural domains can be identified. As shown in Fig. 12, most failure occurrences correspond to the third domain, where tensioned rebars yield, and concrete compressive strains reach the guideline threshold of 0.0035. However, for square-shaped sections, certain weak beam configurations cause flexural capacity to be reached in domain 2 — an uncommon outcome in column design. In this domain, adjacent ground-floor columns experience significantly higher tensile demands than compressive ones, exhibiting a beam-like behavior.

4.4. Tradeoffs between beam and column stiffness

The RC beam optimized in Ref. [21] had clamped-clamped supports, corresponding to columns with infinite moment of inertia; the optimized APM design had a reduced moment of inertia (weak beam), which enhanced CA capacity. In the present study, square section columns restricted the cost-effectiveness of greater moments of inertia for these vertical elements; optimal APM design solutions relate to almost maximum beam moment of inertia due to significantly smaller column stiffness. The following trend is observed: as the optimal depth of elements in a specific direction increases, the depth of elements in the perpendicular direction decreases.

An increase in column moment of inertia enhances its flexural capacity. When addressing rectangular and squared sections of identical manufacturing costs, area and number of rebars, Fig. 12 shows that a rectangular option has a greater resisting envelope due to its greater moment of inertia. Thus, increased column flexural capacity allows greater mobilization of beam CA, which in turn enhances the ultimate load-carrying capacity for (weaker) beams with reduced beam depth. In this context, weaker beams have reduced flexural capacity, even though their CA capacity is greatly improved when paired with highly rigid columns.

This aligns with Long et al. [17], who show that load capacity of frames under CA strongly depends on the moment capacity of the adjacent columns in order to provide strong restraints. This also goes in line with Yu and Tan [16], who show that larger (beam) span-to-depth ratios enhance CA capacity, while smaller ratios improve CAA capacity.

As shown in Section 4.2, lower column moments of inertia create a tradeoff between load-carrying capacity and frame ductility. With weaker lateral restraints, axial forces from CA induce larger horizontal drifts in adjacent columns (weaker beams in Figs. 10 and 11). Consequently, vertical drifts increase at lower loads (Fig. 4b). However, Fig. 4a shows that there is no such tradeoff when strong lateral restraints are available, as increased beam ductility due to CA also implies greater load-carrying capacity. Stronger lateral restraints reduce column horizontal drift, necessitating higher vertical forces for greater vertical drifts.

Therefore, the tradeoff between ultimate capacity and frame ductility displayed in Fig. 8 relates to a specific condition of square columns, which have small moment of inertia. However, different tradeoff behaviors emerge when beam and column stiffness are fully considered (Fig. 13). For these plots, 2000 sample points for the case-study frame were run in OpenSees, with 3 rebars of 20 mm for both beam layers, 20 mm rebars in the columns, and similar materials for the whole frame ($f'_c = 45$ MPa and $f_y = 510$ MPa). Rectangular cross-sections are assumed for beams and columns (width of 300 mm in both), with only their depth varying. For each point, ultimate capacity at CA and the corresponding drift are obtained via FEM.

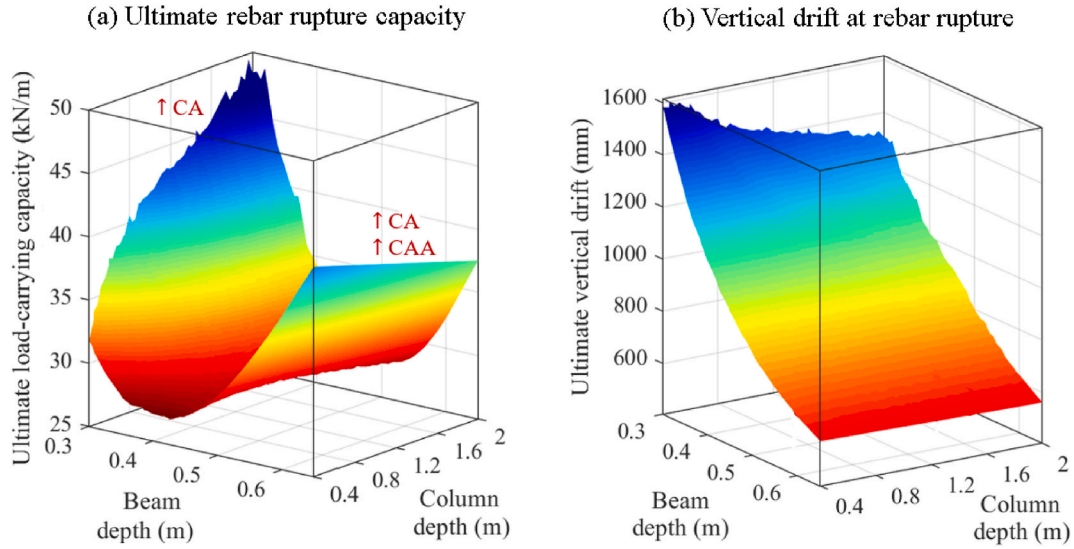


Fig. 13. Ultimate frame capacity at CA in terms of beam depth and column depth.

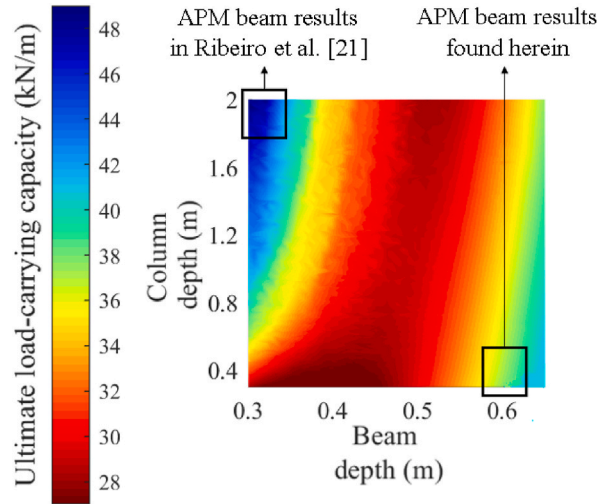


Fig. 14. APM beam results found herein and in Ref. [21] in terms of ultimate capacity.

Ultimate CA capacity reaches its highest values in two scenarios: (a) weak beam with strong columns; and (b) strong beam with weak columns. Although the first combination relates to the greatest CA capacity, it significantly reduces CAA capacity (Fig. 4a). In contrast, the second setup enables a more pronounced CAA mechanism before CA occurs. However, CA in this case is brief, exhibiting much lower ductility (Figs. 4b, 9 and 13b). For a column depth twice its width, ultimate capacities for strong and weak beams become equivalent. Increasing values of column depth leads to CA capacity of weak beams up to $\sim 39\%$ greater than strong beams. Besides, greater column moment of inertia leads simultaneously to greater ductility and CA capacity for weaker beams, resembling the behavior in Fig. 4a and results in Ref. [21].

Intermediate beams are suboptimal in terms of post-flexural resisting mechanisms, as they fail to develop significant compressive forces during CAA and tensile forces during CA. This explains the difference between the optimal design solutions found in Ref. [21] and those presented herein (Fig. 14).

Since critical columns behave like beams in column loss scenarios, reinforcement strategies should specifically account for this behavior. Greater cost-effectiveness is expected if primary frames in column loss scenarios use columns with increased depth and reduced width. However, this may not hold for 3D frames, where significant bending moments occur along both column axes. In such cases, squared, L-shaped, or T-shaped cross-sections may be more cost-effective, a topic for future investigations.

5. Conclusions

This work addressed the optimal risk-based design of a reinforced concrete (RC) frame under progressive collapse caused by external, penultimate, antepenultimate and middle column loss scenarios. Damage leading to loss of load-bearing elements in RC frames are low-probability/high consequence events, with significant impacts in terms of disproportionate collapse consequences and in terms of strengthening costs. Herein, the Alternative Path Method (APM) has been addressed under accidental column loss scenarios, considering multiple strengthening options and distinct column loss scenarios in a planar frame structure. The risk-based optimization looks for a proper point of balance between APM strengthening costs and expected costs of progressive collapse.

Analysis results allow the following conclusions to be drawn:

- Cost-effectiveness of progressive collapse mitigation strategies in RC frames has been found to strongly depend on the tradeoff between beam and column stiffness, as well as on the probability of column loss.
- For columns with squared cross-sections, ensuring great column bending capacity is not cost-effective; hence, ultimate capacity solely relies on increasing beam stiffness to promote compressive arch action. This approach leads to beams of depth twice its width, keeping the expected abnormal load within the compressive arch action range and preventing the onset of catenary action.
- As demonstrated in a previous investigation by the authors, beams with low stiffness, such as those with square cross-sections, can be the most cost-effective solution for alternative load path mechanisms when paired with columns that possess sufficient bending capacity and stiffness to anchor the development of catenary action in the beams.
- For this configuration to be effective in the case-study frame, the column depth must be at least twice that of the square beam depth, with performance improving as the column depth increases. This design approach reveals strong parallels with the “weak beam–strong column” philosophy commonly adopted in seismic design. Such alignment indicates that multi-hazard optimization may be attainable through integrated design strategies, although further research is needed to fully explore and validate this potential.
- Alternative combinations, such as rectangular beams and columns, are shown to be suboptimal in terms of ultimate capacity.

The preference for strengthening beam stiffness over column stiffness, particularly in the case study square column frame, should be interpreted within the specific context and assumptions of this study. Results reflect the case study investigated, including its particular geometric configurations, material properties, and design parameters. As such, it is not intended as a universal guideline but rather as a case-dependent outcome based on the optimization framework and strengthening strategies employed. Other frame aspect ratios are addressed in [62]. Alternative reinforcement techniques and structural configurations, especially those considering different axial compression ratios, reinforcement ratios, or advanced strengthening methods [6,14,22–26], may lead to different cost-benefit conclusions. Thus, while the probability of local damage is treated generically, different hazards may cause distinct damage patterns or affect multiple members simultaneously, which are conditions not captured in the current framework.

Optimal compromise solutions involving beam and column stiffness were discussed, and opportunities for further developments were identified. Possible future developments are the consideration of 3D resisting mechanisms, multi-hazard and threat-dependent scenarios, cost-benefit analysis for tall structures, joint detailing strategies, and usage of hybrid materials.

CRedit authorship contribution statement

Lucas da Rosa Ribeiro: Writing – original draft, Visualization, Software, Investigation, Formal analysis, Data curation, Conceptualization. **Lucas Araújo Rodrigues da Silva:** Formal analysis, Software. **André Teófilo Beck:** Writing – review & editing, Validation, Supervision, Project administration, Methodology, Investigation, Funding acquisition, Formal analysis, Conceptualization. **Fulvio Parisi:** Writing – review & editing, Validation, Supervision, Project administration, Methodology, Investigation, Funding acquisition, Formal analysis, Conceptualization.

Authorship statement

The authors hereby confirm that they are the sole liable persons responsible for the authorship of this work, and that all material that has been herein included as part of the present paper is either the property (and authorship) of the authors, or has the owners' permission to be included here.

Declaration of competing interest

I hereby declare that, to the authors' knowledge, no conflicts of interest in terms of either financial or personal relationships undermine the objectivity, credibility and validity of the research findings presented in the manuscript.

Acknowledgements

Funding of this research project by Brazilian agencies CAPES (Brazilian Higher Education Council), CNPq (Brazilian National Council for Research, grant n. 305010/2024-7), joint FAPESP-ANID (São Paulo State Foundation for Research - Chilean National Agency for Research and Development, grant n. 2019/13080-9), and FAPESP (grants n. 2019/23531-8, 2021/12884-7, 2022/08009-6, 2024/03848-5) is gratefully acknowledged. Also, this study was developed within FAIL-SAFE project (“near-real-time perFormance Assessment of exIsting buiLdings Subjected to initAl Failure through multi-scalE simulation and structural health monitoring”, Grant No. P2022X7N2S_002, CUP N. E53D23003350006), which was funded by European Union through Next-GenerationEU programme - National Recovery and Resilience Plan (PNRR) - Mission 4, Component 2, Investment 1.1, PRIN 2022 programme of the Italian Ministry of University and Research (D.D. February 02, 2022, n.104; PI: Fulvio Parisi).

APPENDIX A

Figure A.1 shows the concrete and steel constitutive models, as discussed in Section 3.4. Figures A.2 to A.5 show the optimal reliability indices corresponding to conventional design, under normal loading conditions, and corresponding to APM-oriented designs, under different column loss scenarios. Results are discussed in Section 4.1 and elsewhere. Figure A.6 shows validation [16,59,60] for the nonlinear structural analysis conducted on OpenSees, disregarding tridimensional effects [5,23,61] in order to fully focus on the planar system [62]. Figure A.7 shows convergence of probabilities of failure obtained via WASM for increasing number of sample points. Figure A.8 shows how static pushdown curves are estimated via surrogates. Figure A.9 show statistical evidence for optimal results. Tables A.1 to A.5 show detailed results of risk-based optimization.

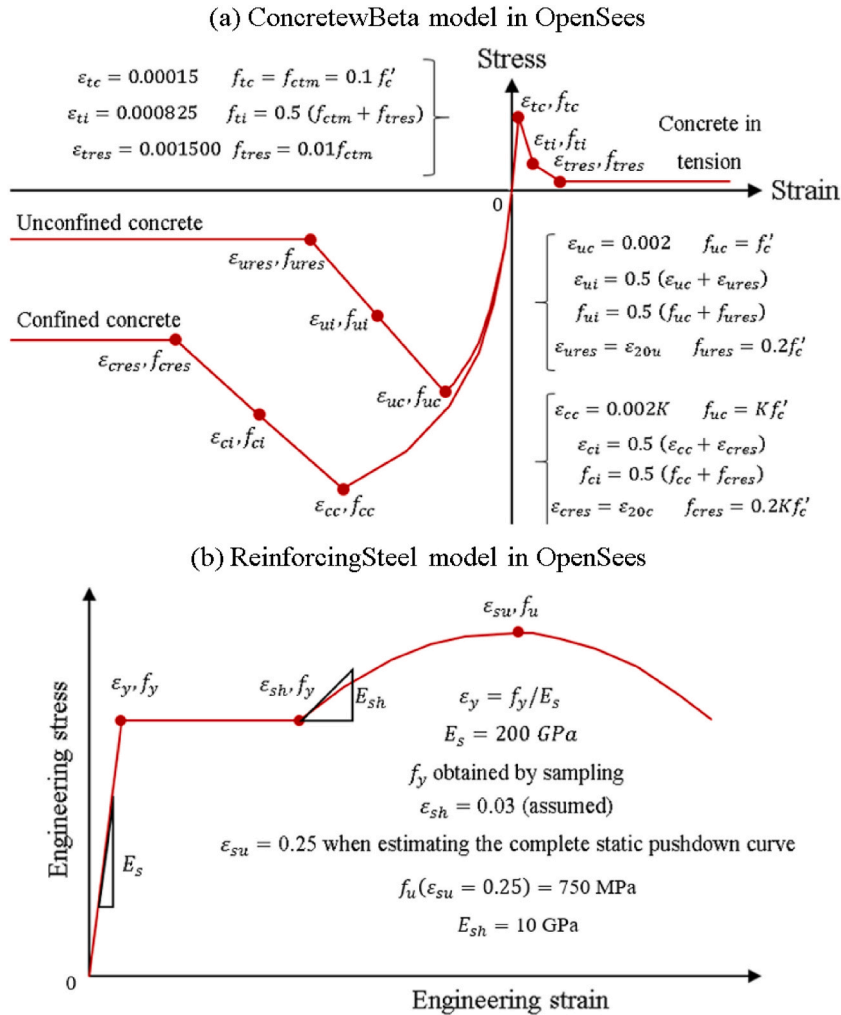


Fig. A.1. Constitutive models and parameter values for concrete (a) and rebars (b).

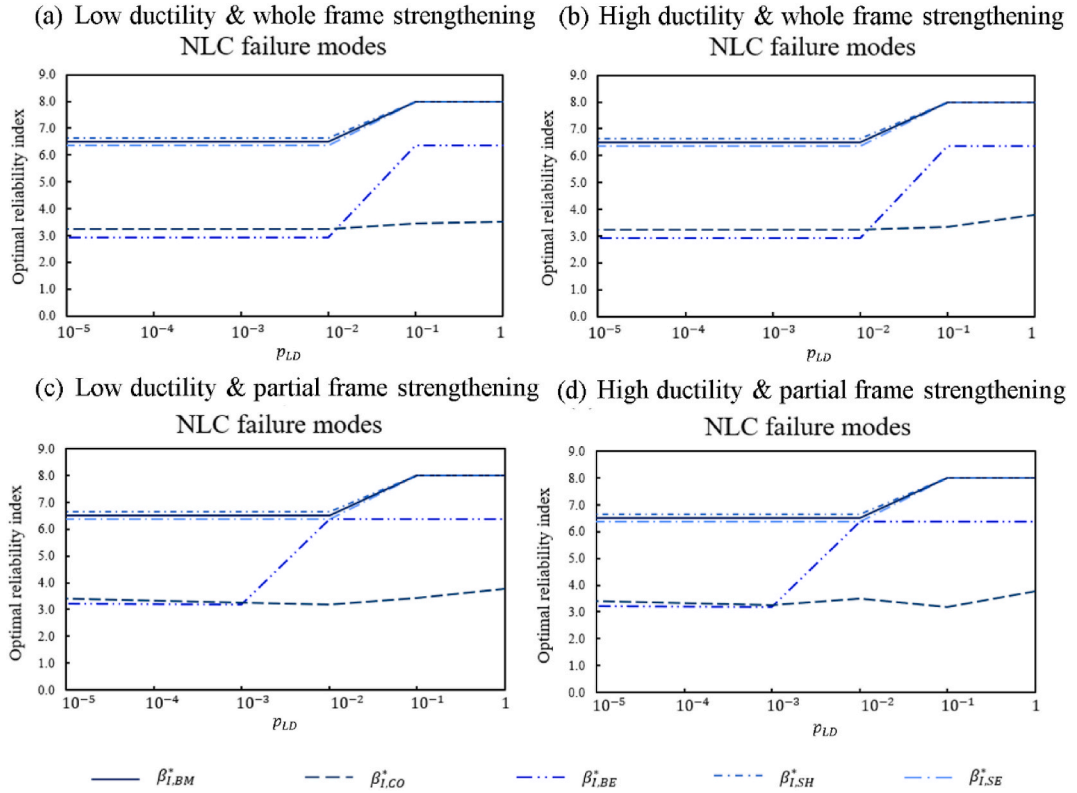


Fig. A.2. Behavior of reliability indices β^* with p_{LD} for Normal Loading Condition (NLC).

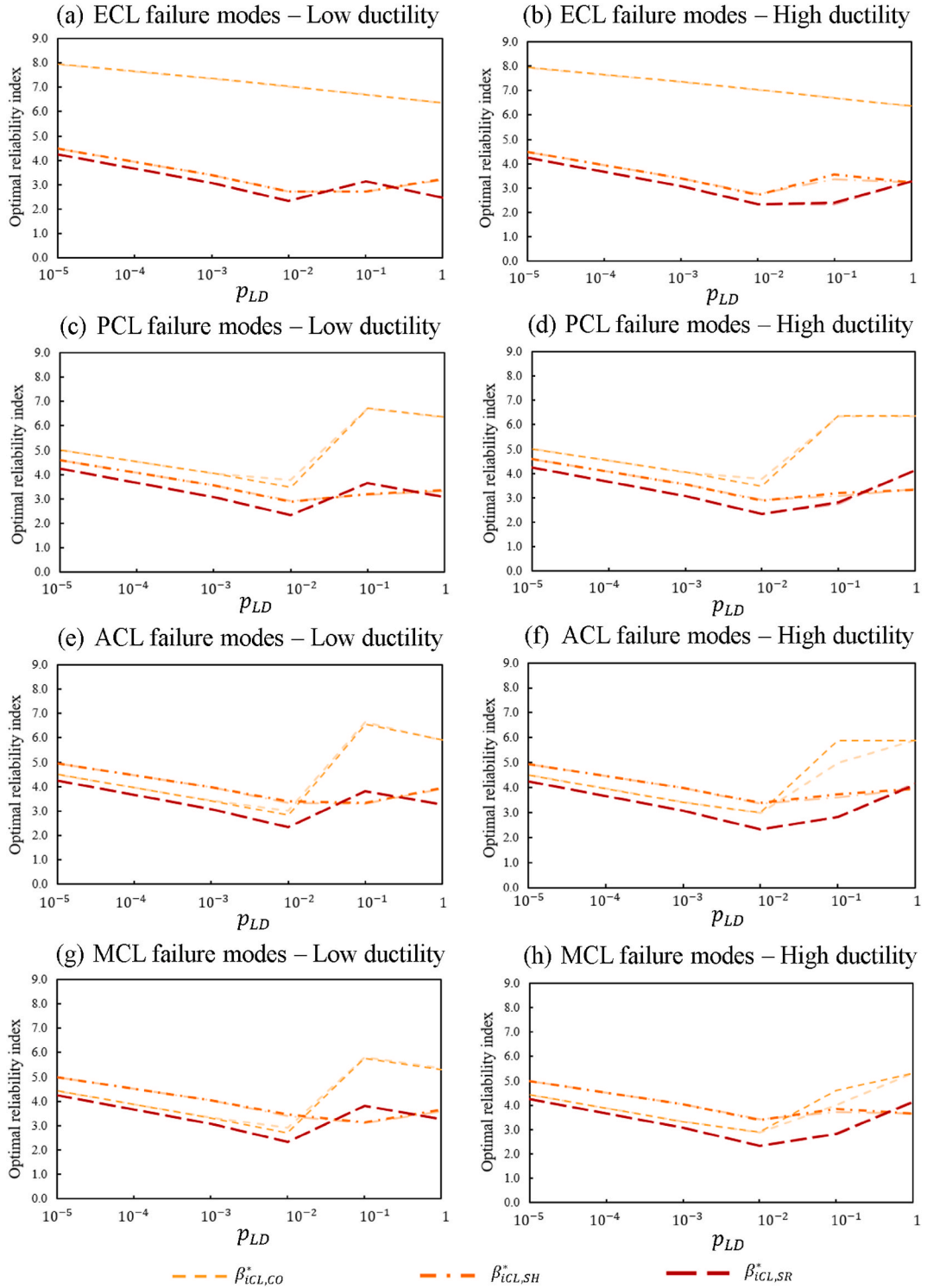


Fig. A.3. Behavior of β^* with p_{LD} for each column loss scenario (whole frame strengthening). Individual column loss in strong lines, and any column loss in thinner lines.

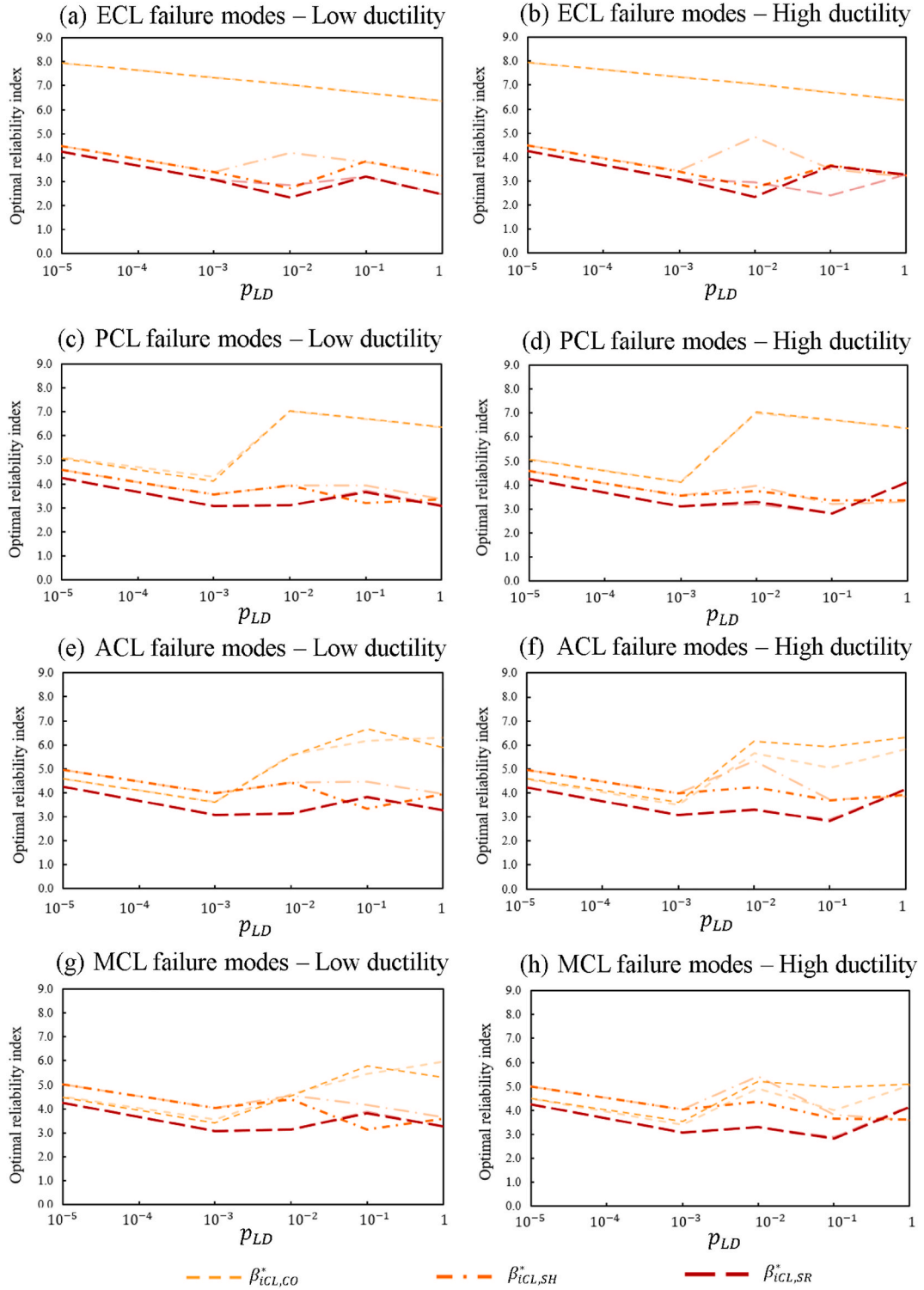


Fig. A.4. Behavior of β^* with p_{LD} for each column loss scenario (partial frame strengthening). Individual column loss in strong lines, and any column loss in thinner (shadow) lines.

Optimal resistance factors γ_{iCL}^* are used to address, via adimensional terms, the capacity increase at each p_{LD} and column loss scenario in terms of the NLC-oriented optimal design:

$$\gamma_{iCL, fm}^* = \frac{R_{iCL, fm}^*(p_{LD})}{R_{iCL, fm}^*(p_{LD}^{min})} \quad (A.1)$$

where iCL is the column loss scenario being addressed; fm is the failure mode being addressed; $R_{iCL, fm}^*(p_{LD})$ relates to the optimal resisting capacity of fm at iCL and p_{LD} . Optimal values of γ_{iCL}^* are shown in Figure A.5 and discussed in Section 4.1.

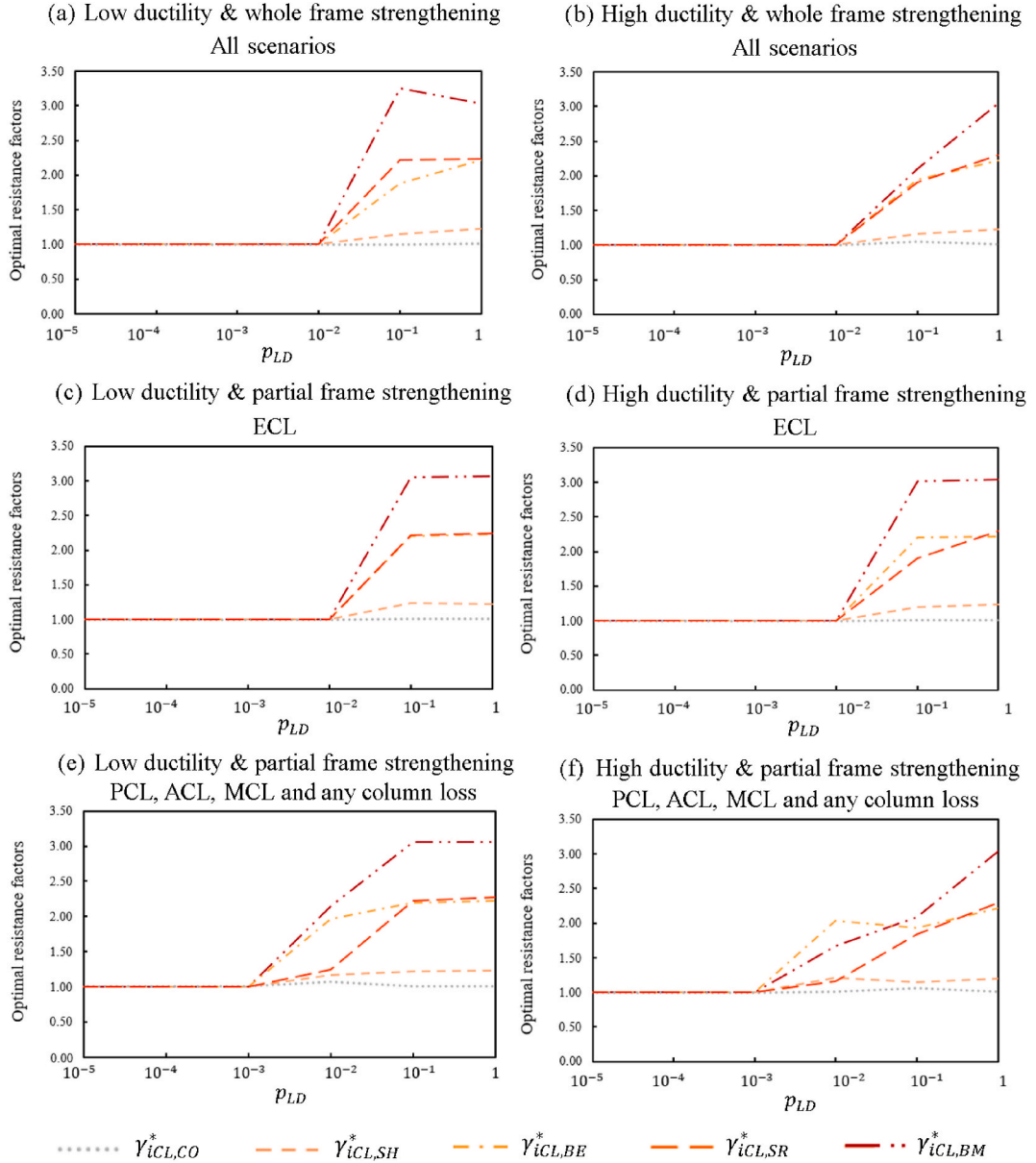


Fig. A.5. Behavior of design factors γ_{iCL}^* with p_{LD} .

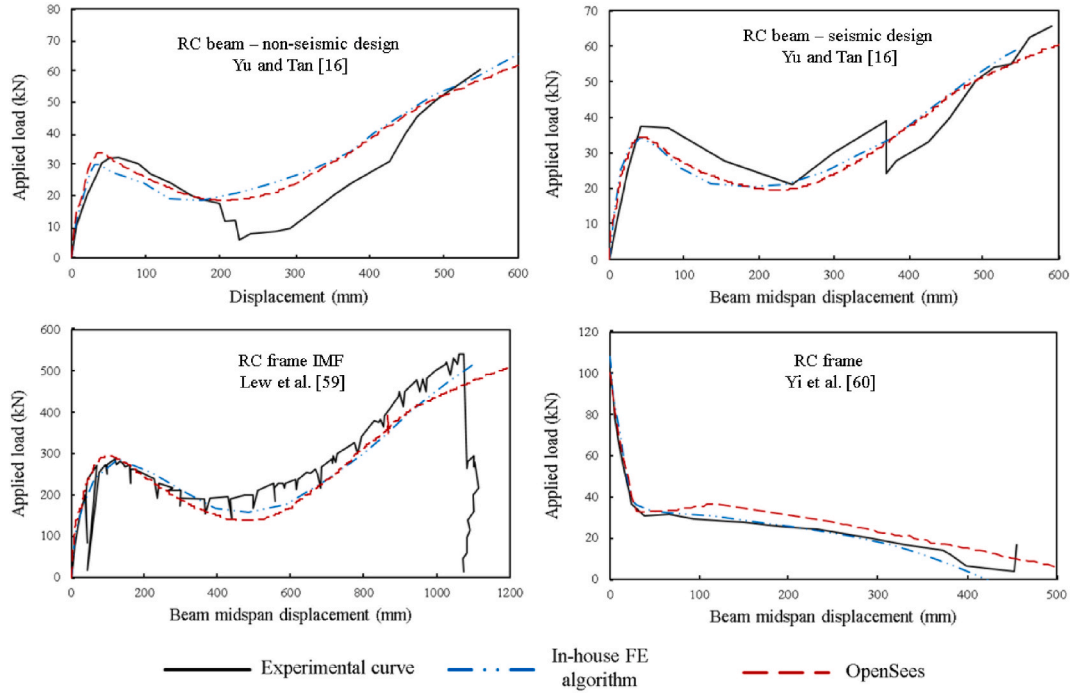


Fig. A.6. Validation for nonlinear structural analysis for column loss scenarios.

Since too many scenarios and strengthening options are used, and a broad design domain is adopted, convergence shown in Figure A.7 relates to the optimal solution for whole frame strengthening at $p_{LD} = 1$ for middle column loss scenario, only for rebar rupture. Only beam depth is chosen to vary, with smaller values related to higher probabilities and higher values leading to smaller probabilities. As it can be seen, convergence becomes evident between 15 and 20 million sample points.

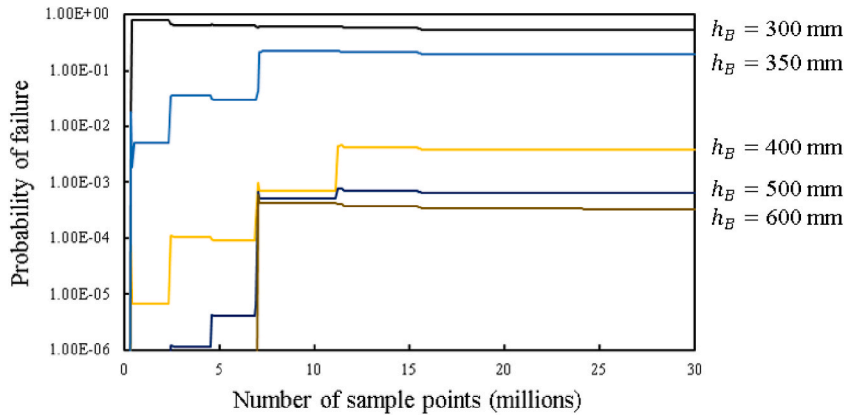


Fig. A.7. Probability of failure convergence (optimal solution at $p_{LD} = 1$, whole frame strengthening, high ductility rebars, middle column loss scenario, varying beam depth from lower to upper bound, addressing only rebar rupture at column loss scenario).

Figure A.8 shows how the static pushdown curve is approximated in the surrogate stage, considering the reference pushdown curve of Fig. 2. Such approximation is needed to reduce computational cost, as for each key point internal forces and corresponding force vs displacement must be estimated for each column loss scenario. A total of 8 key points with representative ε_{su} values are chosen. For our purposes, such values are shown to be adequate for all sampling cases, but other values could be better suited for different structures. An additional ε_{sy} is also treated as a key point, but since it relates to rebar yielding, it varies for each sampling point since f_y is a random variable.

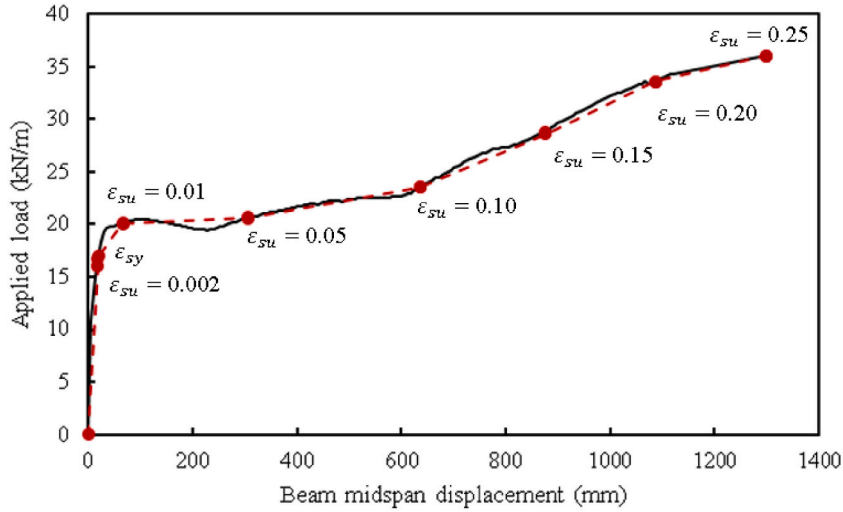


Fig. A.8. Static pushdown curve approximation.

To illustrate variability in the risk-based optimization runs, Figure A.9 shows all optimal solutions found for 10 optimization runs for $p_{LD} = 1$, whole frame strengthening, high ductility rebars, and middle column loss scenario. Too many scenarios, strengthening cases, and p_{LD} values are addressed herein, so just this representative case is shown. Yet, behavior shown in Figure A.9 is similar for all other cases, leading to $\text{CoV} < 5\%$ (error between each individual solution and average solution).

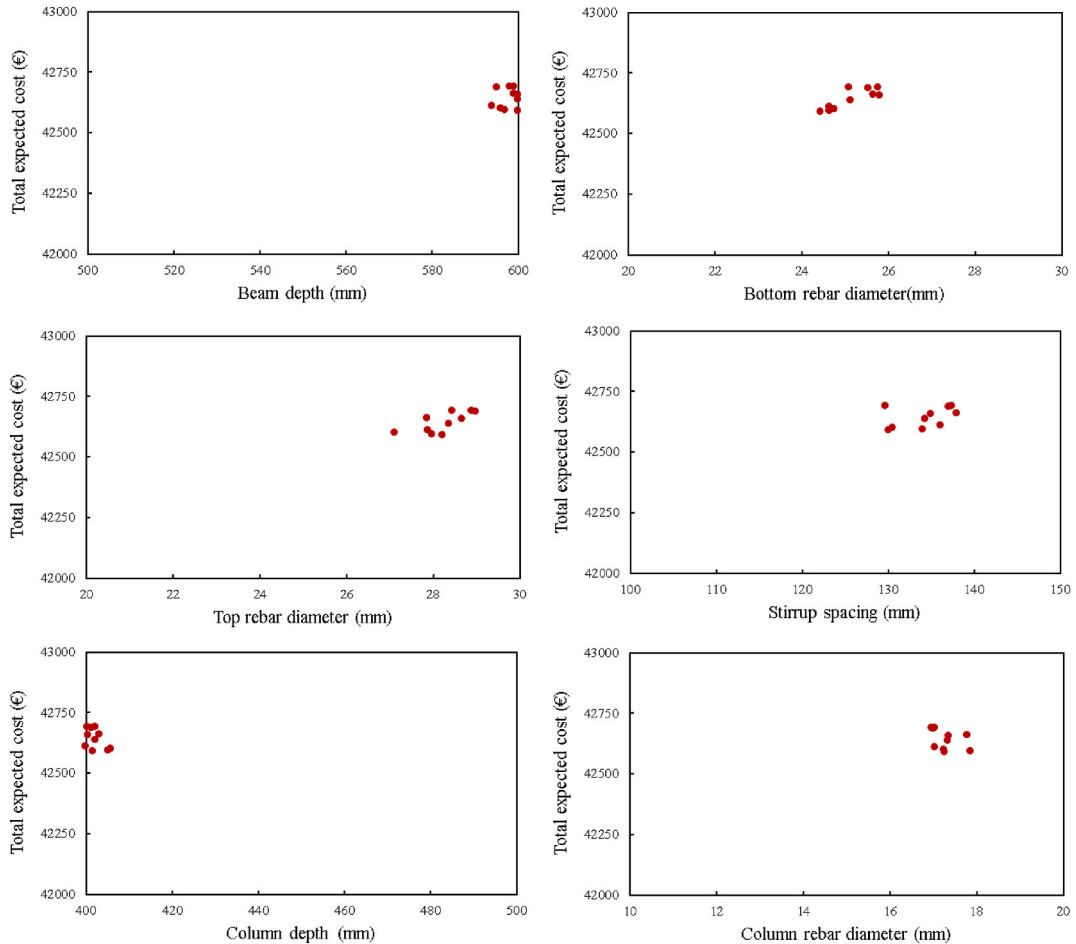


Fig. A.9. Observed variability in risk-optimization results ($p_{LD} = 1$, whole frame strengthening, high ductility rebars, middle column loss scenario).

Table A.1

Optimal risk-based design for each individual scenario of column loss, low ductility rebars and whole frame strengthened.

Scenario	p_{LD}	h_B^* (mm)	ϕ_B^* (mm)	ϕ_T^* (mm)	s_t^* (mm)	h_C^* (mm)	ϕ_C^* (mm)	C_{TE}^* (€)	C_M^* (€)	C_{Beam}^* (€/m)	C_{column}^* (€/m)
External column loss (ECL)	$\leq 10^{-3}$	576	14	19	200	400	16	30741.33	30389.03	83.78	127.14
	10^{-2}	576	14	19	200	400	16	33287.39	30389.02	83.78	127.14
	10^{-1}	588	26	26	149	400	17	42412.93	40923.34	140.96	129.15
	1	598	25	28	134	400	17	44390.52	42354.93	147.17	131.75
Penult. column loss (PCL)	$\leq 10^{-3}$	576	14	19	200	400	16	30743.50	30389.03	83.78	127.14
	10^{-2}	576	14	19	200	400	16	34522.53	30389.02	83.78	127.14
	10^{-1}	590	26	26	148	400	17	41565.87	40996.14	141.25	129.32
	1	600	25	28	135	400	17	43230.63	42537.87	147.51	132.76
Antepenult. column loss (ACL)	$\leq 10^{-3}$	576	14	19	200	400	16	30743.50	30389.03	83.78	127.14
	10^{-2}	581	14	19	199	400	16	36942.24	30806.65	85.49	128.05
	10^{-1}	589	26	26	149	400	17	41361.58	40956.93	141.04	129.30
	1	600	25	28	139	400	17	42639.68	42306.72	147.13	131.42
Middle column loss (MCL)	$\leq 10^{-3}$	576	14	19	200	400	16	30744.28	30389.03	83.78	127.14
	10^{-2}	580	14	19	200	400	16	31584.05	30820.03	85.66	127.92
	10^{-1}	587	26	26	149	400	17	41202.75	40968.68	141.19	129.19
	1	600	25	28	135	406	17	42634.67	42513.72	147.33	132.79

Table A.2

Optimal risk-based design for each column loss scenario, high ductility rebars and whole frame strengthened

Scenario	p_{LD}	h_B^* (mm)	ϕ_B^* (mm)	ϕ_T^* (mm)	s_t^* (mm)	h_C^* (mm)	ϕ_C^* (mm)	C_{TE}^* (€)	C_M^* (€)	C_{Beam}^* (€/m)	C_{column}^* (€/m)
External column loss (ECL)	$\leq 10^{-3}$	576	14	19	200	401	16	30994.74	30389.03	83.78	127.14
	10^{-2}	576	14	19	200	401	16	33287.33	30389.02	83.78	127.14
	10^{-1}	597	20	26	151	412	16	39314.92	38250.37	125.15	130.59
	1	600	25	28	137	412	17	42885.04	42490.03	147.03	133.10
Penult. column loss (PCL)	$\leq 10^{-3}$	576	14	19	200	401	16	31118.25	30389.03	83.78	127.14
	10^{-2}	576	14	19	200	401	16	34522.48	30389.02	83.78	127.14
	10^{-1}	595	20	26	157	413	17	39413.46	38050.66	123.32	131.67
	1	600	25	28	138	413	17	42696.26	42338.31	146.86	132.08
Antepenult. column loss (ACL)	$\leq 10^{-3}$	576	14	19	200	401	16	31428.39	30389.03	83.78	127.14
	10^{-2}	584	14	19	199	400	17	36062.45	31214.29	85.58	131.31
	10^{-1}	600	20	26	157	408	17	39061.80	38257.98	124.16	132.14
	1	600	25	28	135	408	17	42592.19	42497.36	147.33	132.71
Middle column loss (MCL)	$\leq 10^{-3}$	576	14	19	200	401	16	31583.99	30389.03	83.78	127.14
	10^{-2}	581	14	19	200	401	17	36921.59	31376.24	86.40	131.44
	10^{-1}	597	20	26	153	406	17	39135.82	38330.48	125.18	131.21
	1	600	25	28	134	406	17	42634.67	42513.72	147.38	132.77

Table A.3

Optimal risk-based design for each individual scenario of column loss, low ductility rebars and strengthening in the 2 first floors.

Scenario	p_{LD}	h_B^* (mm)	ϕ_B^* (mm)	ϕ_T^* (mm)	s_t^* (mm)	h_C^* (mm)	ϕ_C^* (mm)	C_{TE}^* (€)	C_M^* (€)	C_{Beam}^* (€/m)	C_{column}^* (€/m)
External column loss (ECL)	$\leq 10^{-3}$	576	14	19	200	401	16	31294.79	30388.91	83.78	127.14
	10^{-2}	576	14	19	200	400	16	33913.41	30392.91	83.78	127.18
	10^{-1}	600	25	28	135	400	17	43058.98	34243.77	146.84	132.99
	1	600	25	28	137	400	17	44768.34	34898.23	147.31	132.75
Penult. column loss (PCL)	$\leq 10^{-3}$	576	14	19	200	401	16	30685.62	30069.02	84.13	127.75
	10^{-2}	600	20	26	153	402	16	33836.69	33188.65	125.77	130.28
	10^{-1}	589	26	26	147	400	17	34820.34	34257.38	141.33	130.20
	1	600	25	28	134	401	17	35534.19	34832.16	147.04	132.59
Antepenult. column loss (ACL)	$\leq 10^{-3}$	576	14	19	200	401	16	30784.62	30174.30	84.52	129.35
	10^{-2}	591	21	26	151	405	17	33586.22	33088.29	124.58	129.96
	10^{-1}	590	26	26	148	400	17	34638.90	34247.30	141.13	129.29
	1	600	25	28	134	401	17	35149.26	34868.60	147.46	132.72
Middle column loss (MCL)	$\leq 10^{-3}$	576	14	19	200	401	16	31061.62	30112.47	84.71	129.23
	10^{-2}	600	20	26	153	401	16	33721.38	33142.14	125.73	130.34
	10^{-1}	590	26	26	148	401	17	34911.80	34250.85	146.49	132.60
	1	600	25	28	139	401	17	35142.90	34785.19	147.56	132.78

Table A.4

Optimal risk-based design for each column loss scenario, high ductility rebars and strengthening in the 2 first floors

Scenario	p_{LD}	h_B^* (mm)	ϕ_B^* (mm)	ϕ_T^* (mm)	s_t^* (mm)	h_C^* (mm)	ϕ_C^* (mm)	C_{TE}^* (€)	C_M^* (€)	C_{Beam}^* (€/m)	C_{column}^* (€/m)
External column loss (ECL)	$\leq 10^{-3}$	576	14	19	200	401	16	30568.72	30066.57	84.12	127.71
	10^{-2}	576	14	19	200	400	16	32913.38	30015.60	83.78	127.15
	10^{-1}	595	25	28	140	400	17	34865.69	34690.66	146.29	130.77
	1	600	25	28	135	400	17	35238.62	34853.04	147.24	132.73
Penult. column loss (PCL)	$\leq 10^{-3}$	576	14	19	200	401	16	30685.56	30069.01	84.13	127.75
	10^{-2}	600	19	27	138	400	17	33512.69	33204.41	125.36	131.21
	10^{-1}	600	20	26	153	401	16	34545.96	33192.13	125.82	130.27
	1	600	25	28	135	400	17	35150.65	34876.60	147.53	132.79
Antepenult. column loss (ACL)	$\leq 10^{-3}$	576	14	19	200	401	16	30784.51	30174.04	84.51	129.36
	10^{-2}	599	19	26	151	400	17	33238.40	33028.59	122.19	132.29
	10^{-1}	600	20	26	152	404	17	33993.89	33164.52	124.57	131.56
	1	600	25	28	138	400	17	34914.74	34852.43	147.19	132.79
Middle column loss (MCL)	$\leq 10^{-3}$	576	14	19	200	401	16	30852.53	30174.07	84.51	129.36
	10^{-2}	597	19	27	138	401	17	33443.74	33222.64	124.75	132.50
	10^{-1}	600	20	26	158	400	18	34007.25	33263.91	123.36	135.43
	1	596	25	28	134	402	17	34931.39	34736.58	147.36	130.14

Table A.5

Optimal risk-based design addressing sudden loss at any ground floor column.

Scenario	p_{LD}	h_B^* (mm)	ϕ_B^* (mm)	ϕ_T^* (mm)	s_t^* (mm)	h_C^* (mm)	ϕ_C^* (mm)	C_{TE}^* (€)	C_M^* (€)	C_{Beam}^* (€/m)	C_{column}^* (€/m)
Entire frame strengthened Low ductility	$\leq 10^{-3}$	576	14	19	200	400	16	30740.11	30389.03	83.78	127.14
	10^{-2}	576	14	19	200	401	16	31238.16	30389.03	86.98	130.43
	10^{-1}	582	25	25	198	400	17	35372.65	31360.22	140.86	129.41
	1	589	25	28	152	401	17	41772.35	40935.29	146.78	131.48
Entire frame strengthened Greater ductility	$\leq 10^{-3}$	576	14	19	200	400	16	31238.11	30389.03	83.78	127.14
	10^{-2}	583	14	19	199	400	17	35183.22	31188.82	86.41	129.86
	10^{-1}	595	20	26	160	404	16	39427.41	37782.89	122.73	130.33
	1	600	25	28	136	400	17	42714.02	42486.48	147.25	132.73
Two floors strengthened Low ductility	$\leq 10^{-3}$	576	14	19	200	401	16	30705.37	30182.34	84.71	129.23
	10^{-2}	600	20	26	153	404	16	33839.96	33189.20	125.73	130.34
	10^{-1}	600	25	28	137	400	17	34909.86	34793.04	146.49	132.60
	1	600	25	28	135	400	17	35747.93	34878.20	147.56	132.78
Two floors strengthened Greater ductility	$\leq 10^{-3}$	576	14	19	200	401	16	30785.70	30098.34	84.68	127.54
	10^{-2}	600	18	27	140	400	17	33420.76	33135.32	122.98	133.33
	10^{-1}	595	20	26	156	400	17	34499.01	33108.15	124.40	130.65
	1	600	25	28	144	400	17	35007.08	34683.61	145.78	131.40

Data availability

Data will be made available on request.

References

- [1] F. Parisi, N. Augenti, Influence of seismic design criteria on blast resistance of RC framed buildings: a case study, Eng. Struct. 44 (2012) 78–93, <https://doi.org/10.1016/j.engstruct.2012.05.046>.
- [2] D.E. Allen, W.R. Schriever, Progressive collapse, abnormal loads and building codes, in: Proceedings ASCE National Meeting on Structural Engineering: 1972–04, Cleveland, USA, 1972. <https://nrc-publications.canada.ca/eng/view/ft/?id=3415baa7-5d26-4dc2-9761-36f882596403>.
- [3] J.L. Gross, W. Mcguire, Progressive collapse resistant design, J. Struct. Eng. 109 (1) (1983) 1–15, [https://doi.org/10.1061/\(ASCE\)0733-9445\(1983\)109:1\(1\)](https://doi.org/10.1061/(ASCE)0733-9445(1983)109:1(1)).
- [4] J.M. Adam, F. Parisi, J. Sagaseta, X. Lu, Research and practice on progressive collapse and robustness of building structures in the 21st century, Eng. Struct. 173 (2018) 122–149, <https://doi.org/10.1016/j.engstruct.2018.06.082>.
- [5] N. Elkady, A.L. Nelson, L. Weekes, N. Makooond, M. Buitrago, Progressive collapse: past, present, future and beyond, Structures 62 (2024) 106131, <https://doi.org/10.1016/j.istruc.2024.106131>.
- [6] F. Kiakojouri, V. De Biagi, B. Chiaia, M.R. Sheidaii, Strengthening and retrofitting techniques to mitigate progressive collapse: a critical review and future research agenda, Eng. Struct. 262 (2022) 114274, <https://doi.org/10.1016/j.engstruct.2022.114274>.
- [7] N. Gardner, J. Huh, L. Chung, Lessons from the sampoong department store collapse, Cement Concr. Compos. 24 (6) (2002) 523–529, [https://doi.org/10.1016/S0958-9465\(01\)00068-3](https://doi.org/10.1016/S0958-9465(01)00068-3).
- [8] EUROPEAN COMMITTEE FOR STANDARTIZATION, Eurocode 1: actions on structures – part 1-7: general actions — accidental actions, CEN, EN 1991 (2006). Brussels, Belgium.
- [9] GENERAL SERVICES ADMINISTRATION (GSA), General services administration alternate path analysis & design guidelines for progressive collapse resistance, Washington DC, https://www.gsa.gov/system/files/Progressive_Collapse_2016.pdf, 2016.

- [10] A.T. Beck, L.d.R. Ribeiro, M. Valdebenito, Risk-based cost-benefit analysis of frame structures considering progressive collapse under column removal scenarios, *Eng. Struct.* 225 (2020) 111295, <https://doi.org/10.1016/j.engstruct.2020.111295>.
- [11] A.T. Beck, L.d.R. Ribeiro, M. Valdebenito, H.A. Jensen, Risk-based design of regular plane frames subject to damage by abnormal events: a conceptual study, *J. Struct. Eng.* 148 (1) (2022) 04021229, [https://doi.org/10.1061/\(ASCE\)ST.1943-541X.0003196](https://doi.org/10.1061/(ASCE)ST.1943-541X.0003196).
- [12] M. Sasani, M. Bazan, S. Sagirolu, Experimental and analytical progressive collapse evaluation of actual reinforced concrete structure, *ACI Struct. J.* 104 (6) (2007) 731–739, <https://doi.org/10.14359/18955>.
- [13] C.S.N. Praxedes, Robustness-Based Optimal Progressive Collapse Design of RC Frame Structures, Thesis (PhD – Civil Engineering), Ryerson University, Toronto, Canada, 2020.
- [14] K. Alogla, L. Weekes, L. Augustus-Nelson, A new mitigation scheme to resist progressive collapse of RC structures, *Constr. Build. Mater.* 125 (2016) 533–545, <https://doi.org/10.1016/j.conbuildmat.2016.08.084>.
- [15] I.M. Alshaikh, B.A. Bakar, E.A. Alwesabi, H.M. Akil, Experimental investigation of the progressive collapse of reinforced concrete structures: an overview, *Structures* 25 (2020) 881–900, <https://doi.org/10.1016/j.iistruc.2020.03.018>.
- [16] J. Yu, K.H. Tan, Experimental and numerical investigation on progressive collapse resistance of reinforced concrete beam column sub-assemblies, *Eng. Struct.* 55 (2013) 90–106, <https://doi.org/10.1016/j.engstruct.2011.08.040>.
- [17] X. Long, S. Wang, X.-J. Huang, C. Li, S.-B. Kang, Progressive collapse resistance of exterior reinforced concrete frames and simplified method for catenary action, *Eng. Struct.* 249 (2021) 113316, <https://doi.org/10.1016/j.engstruct.2021.113316>.
- [18] B. Abdelwahed, Beam-column joints reinforcement detailing adequacy in case of a corner column loss-numerical analysis, *Lat. Am. J. Solid. Struct.* 16 (7) (2019) e216, <https://doi.org/10.1590/1679-78255536>.
- [19] A.T. Beck, W.J.S. Gomes, A comparison of deterministic, reliability-based and risk-based structural optimization under uncertainty, *Probab. Eng. Mech.* 28 (2012) 18–29, <https://doi.org/10.1016/j.probenmech.2011.08.007>.
- [20] A.T. Beck, W.J.S. Gomes, R.H. Lopez, L.F.F. Miguel, A comparison between robust and risk-based optimization under uncertainty, *Struct. Multidiscip. Optim.* 52 (2015) 479–492, <https://doi.org/10.1007/s00158-015-1253-9>.
- [21] L. d R. Ribeiro, H.M. Kroetz, F. Parisi, A.T. Beck, Optimal risk-based design of reinforced concrete beams against progressive collapse, *Eng. Struct.* 300 (2024) 117158, <https://doi.org/10.1016/j.engstruct.2023.117158>.
- [22] S. Gao, L. Guo, Z. Zhang, Anti-collapse performance of composite frame with special-shaped MCFST columns, *Eng. Struct.* 245 (2021) 112917, <https://doi.org/10.1016/j.engstruct.2021.112917>.
- [23] V. Makoond, A. Setlwan, M. Bultrago, J.M. Adam, Arresting failure propagation in buildings through collapse isolation, *Nature* 629 (2024) 592–596, <https://doi.org/10.1038/s41586-024-07268-5>.
- [24] S. Gerasimidis, B. Ellingwood, Twenty years of advances in disproportionate collapse research and best practices since 9/11/2001, *J. Struct. Eng.* 149 (2) (2022) 02022002, <https://doi.org/10.1061/JSENDH.STENG-12056>.
- [25] B. Meng, H. Li, J.-Y.R. Liew, S. Li, D.-Y. Kong, Enhancing the collapse resistance of a composite subassembly with fully welded joints using sliding inner cores, *J. Struct. Eng.* 150 (8) (2024) 04024085, <https://doi.org/10.1061/JSENDH.STENG-13418>.
- [26] B. Meng, K. You, B. Yang, D. Kong, J. Wen, Anti-progressive collapse performance and design method of novel T-stub connections, *Eng. Struct.* 319 (2024) 118880, <https://doi.org/10.1016/j.engstruct.2024.118880>.
- [27] K. Khandelwal, S. el-Tawil, Pushdown resistance as a measure of robustness in progressive collapse analysis, *Eng. Struct.* 33 (2011) 2653–2661, <https://doi.org/10.1016/j.engstruct.2011.05.013>.
- [28] D.A. Rodrigues, L.A. Silva, A.J. Torii, A.T. Beck, System-reliability-based sizing and shape optimization of trusses considering millions of failure sequences, *Struct. Saf.* 108 (2024) 102448, <https://doi.org/10.1016/j.strusafe.2024.102448>.
- [29] B.R. Ellingwood, Mitigating risk form abnormal loads and progressive collapse, *J. Perform. Constr. Facil.* 20 (4) (2006) 315–323, [https://doi.org/10.1061/\(ASCE\)0887-3828\(2006\)20:4\(315\)](https://doi.org/10.1061/(ASCE)0887-3828(2006)20:4(315)).
- [30] A.T. Beck, M.G. Stewart, Risk-based cost-benefit analysis of structural strengthening to mitigate disproportionate collapse of buildings under abnormal blast loading, *Structures* 57 (2023) 105103, <https://doi.org/10.1016/j.iistruc.2023.105103>.
- [31] E. Pate-Cornell, Quantitative safety goals for risk management of industrial facilities, *Struct. Saf.* 13 (3) (1987) 145–157, [https://doi.org/10.1016/0167-4730\(94\)90023-X](https://doi.org/10.1016/0167-4730(94)90023-X). Elsevier.
- [32] X.S. Yang, Nature-Inspired Metaheuristic Algorithms, Luniver Press, UK, 2008. https://www.researchgate.net/publication/235979455_Nature-Inspired_Metaheuristic_Algorithms.
- [33] M. Rashki, M. Miri, M.A. Moghaddam, A new efficient simulation method to approximate the probability of failure and most probable point, *Struct. Saf.* 39 (2012) 22–29, <https://doi.org/10.1016/j.strusafe.2012.06.003>.
- [34] M. Rashki, M. Miri, M.A. Moghaddam, Closure to “A new efficient Simulation method to approximate the probability of failure and most probable point”, *Struct. Saf.* 46 (2014) 15–16, <https://doi.org/10.1016/j.strusafe.2013.08.002>.
- [35] F.T. Mckenna, M.H. Scott, G.L. Fenves, Nonlinear finite-element analysis software architecture using object composition, *J. Comput. Civ. Eng.* 24 (1) (2010) 95–107, [https://doi.org/10.1061/\(ASCE\)CP.1943-5487.0000002](https://doi.org/10.1061/(ASCE)CP.1943-5487.0000002). ASCE.
- [36] D. Shepard, A two-dimensional interpolation function for irregularly-spaced data, in: *Proceedings of the 1968 23rd ACM National Conference*, 1968, pp. 517–524, <https://doi.org/10.1145/800186.810616>.
- [37] M.D. McKay, R.J. Beckman, W.J. Conover, Comparison of three methods for selecting values of input variables in the analysis of output from a computer code, *Technometrics* 21 (2) (1979) 239–245, <https://doi.org/10.1080/00401706.1979.10489755>.
- [38] B. Tang, Orthogonal array-based Latin hypercubes, *J. Am. Stat. Assoc.* 88 (424) (1993) 1392–1397, <https://doi.org/10.2307/2291282>.
- [39] K.Q. Ye, Orthogonal column Latin hypercubes and their application in computer experiments, *J. Am. Stat. Assoc.* 93 (444) (1998) 1430–1439, <https://doi.org/10.1080/01621459.1998.10473803>.
- [40] S. Gao, Life cycle sustainability assessment of concrete-filled steel tubular frames in earthquake regions, *Eng. Struct.* 328 (2025) 119761, <https://doi.org/10.1016/j.engstruct.2025.119761>.
- [41] SINAPI (Sistema Nacional de Pesquisa de Custos e Índices da Construção Civil), Reference for prices and costs [In Portuguese]. [Referência de preços e custos], <https://www.caixa.gov.br/poder-publico/modernizacao-gestao/sinapi/Paginas/default.aspx>, 2024. (Accessed 31 March 2025).
- [42] BANCO CENTRAL DO BRASIL, Currency converter [In Portuguese]. [Conversor de moedas], <https://www.bcb.gov.br/conversao>, 2024. (Accessed 31 March 2025).
- [43] K.E. Marchand, D.J. Stevens, Progressive collapse criteria and design approaches improvement, *J. Perform. Constr. Facil.* 29 (5) (2015) B4015004, [https://doi.org/10.1061/\(ASCE\)CF.1943-5509.0000706](https://doi.org/10.1061/(ASCE)CF.1943-5509.0000706).
- [44] AMERICAN CONCRETE INSTITUTE (ACI), ACI 318-19: Building Code Requirements for Structural Concrete, Detroit, Michigan, 2019, <https://doi.org/10.14359/51716937>.
- [45] JOINT COMMITTEE ON STRUCTURAL SAFETY (JCSS), Probabilistic model code: part 3: material properties. <https://www.jcss-lc.org/jcss-probabilistic-model-code/>, 2002.
- [46] F. Parisi, M. Scalvenzi, E. Brunesi, Performance limit states for progressive collapse analysis of reinforced concrete framed buildings, *Struct. Concr.* 20 (2019) 68–84, <https://doi.org/10.1002/suco.201800039>.
- [47] Wisniewski, D.; Cruz, P. J. S.; Henriques, A. A.; Simões, R. A. D. Probabilistic models for mechanical properties of concrete, reinforcing steel and pre-stressing steel. *Struct. Infrastr. Eng.*, v. 8, n. 2, p. 111–123. <https://doi.org/10.1080/15732470903363164>.
- [48] C. Galasso, G. Maddaloni, E. Cosenza, Uncertainty analysis of flexural overstrength for capacity design of RC beams, *J. Struct. Eng.* 140 (7) (2014) 04014037, [https://doi.org/10.1061/\(ASCE\)ST.1943-541X.0001024](https://doi.org/10.1061/(ASCE)ST.1943-541X.0001024).
- [49] B. Ellingwood, T.V. Galambos, Probability-based criteria for structural design, *Struct. Saf.* 1 (1) (1982) 15–26, [https://doi.org/10.1016/0167-4730\(82\)90012-1](https://doi.org/10.1016/0167-4730(82)90012-1).

- [50] R. Park, M.J.N. Priestley, W.D. Gill, Ductility of square-confined concrete columns, *J. Struct. Eng.* 108 (ST4) (1982) 929–950, <https://doi.org/10.1061/JSDAAG.0005933>.
- [51] COMITÉ EURO-INTERNATIONAL DU BÉTON, CEB-FIP. Model Code 2010: Final Draft, Bulletin D'information, CEB, Lausanne, 2011, <https://doi.org/10.35789/fib.BULL.0066>.
- [52] B.A. Izzuddin, A.G. Vlassis, A.Y. Elghazouli, D.A. Nethercot, Progressive collapse of multi-storey buildings due to sudden column loss - part I: simplified assessment framework, *Eng. Struct.* 30 (5) (2008) 1308–1318, <https://doi.org/10.1016/j.engstruct.2007.07.011>.
- [53] G.Q. Xu, B.R. Ellingwood, An energy-based partial pushdown analysis procedure for assessment of disproportionate collapse potential, *J. Constr. Steel Res.* 67 (3) (2011) 547–555, <https://doi.org/10.1016/j.jcsr.2010.09.001>.
- [54] B. Xue, J.L. le, Simplified energy-based analysis of collapse risk of reinforced concrete buildings, *Struct. Saf.* 63 (2016) 47–58, <https://doi.org/10.1016/j.strusafe.2016.07.003>. Elsevier.
- [55] Y. Bao, J.A. Main, S.-Y. Noh, Evaluation of structural robustness against column loss: methodology and application to RC frame buildings, *J. Struct. Eng.* 143 (8) (2017) 04017066, [https://doi.org/10.1061/\(ASCE\)ST.1943-541X.0001795](https://doi.org/10.1061/(ASCE)ST.1943-541X.0001795).
- [56] P. Ren, Y. Li, X. Lu, H. Guan, Y. Zhou, Experimental investigation of progressive collapse resistance of one-way reinforced concrete beam-slab substructures under a middle column-removal scenario, *Eng. Struct.* 118 (2016) 28–40, <https://doi.org/10.1016/j.engstruct.2016.03.051>.
- [57] C.S.N. Praxedes, X.-X. Yuan, Robustness-oriented optimal design for reinforced concrete frames considering the large uncertainty of progressive collapse threats, *Struct. Saf.* 94 (2022) 102139, <https://doi.org/10.1016/j.strusafe.2021.102139>. Elsevier.
- [58] M.G. Stewart, S. Thöns, A.T. Beck, Assessment of risk reduction strategies for terrorist attacks on structures, *Struct. Saf.* 104 (2023) 102353, <https://doi.org/10.1016/j.strusafe.2023.102353>.
- [59] H.S. Lew, Y. Bao, S. Pujol, M.A. Sozen, Experimental study of reinforced concrete assemblies under column removal scenario, *ACI Struct. J.* 111 (4) (2014) 881–892, <https://doi.org/10.14359/51686739>.
- [60] W.-J. Yi, Q.-F. He, Y. Xiao, S.K. Kunnath, Experimental study on progressive collapse resistant behavior of reinforced concrete frame structures, *ACI Struct. J.* 105 (4) (2008) 433–439, <https://doi.org/10.14359/19857>.
- [61] S. Gao, L. Guo, Progressive collapse analysis of 20-storey building considering composite action of floor slab, *Int. J. Steel Struct.* 15 (2015) 447–458, <https://doi.org/10.1007/s13296-015-6014-5>.
- [62] L.R. Ribeiro, F.C. Macedo, A.T. Beck, F. Parisi, Optimal risk-based design of planar RC frames under progressive collapse: influence of frame aspect ratio and column cross-section, *Engineering Structures* 342 (2025) 120905. <https://doi.org/10.1016/j.engstruct.2025.120905>.